Title: Structural connectivity matures along a sensorimotor-association connectional axis in youth

Authors: Xiaoyu Xu[1,2], Hang Yang[2], Jing Cong[1,2], Valerie Sydnor[3], Zaixu Cui[2*]

Affiliations:

[1]State Key Laboratory of Cognitive Neuroscience and Learning, Beijing Normal University; Beijing, 100875, China.

[2]Chinese Institute for Brain Research, Beijing; Beijing, 102206, China.

[3]Department of Psychiatry, University of Pittsburgh Medical Center; Pittsburgh, PA, USA.

[*]Correspondence: cuizaixu@cibr.ac.cn

Abstract

Childhood and adolescence are associated with protracted developmental remodeling of cortico-cortical structural connectivity. However, how heterochronous development in white matter structural connectivity spatially and temporally unfolds across the macroscale human connectome remains unknown. Leveraging non-invasive diffusion MRI data from both cross-sectional (N = 590) and longitudinal (baseline: N = 3,949; two-year follow-up: N = 3,155) developmental datasets, we found that structural connectivity development diverges along a pre-defined sensorimotor-association (S-A) connectional axis from ages 8.1 to 21.9 years. Specifically, we observed a continuum of developmental profiles that spans from an early childhood increase in connectivity strength in sensorimotor-sensorimotor connections to a late adolescent increase in association-association connectional strength. The S-A connectional axis also captured spatial variations in associations between structural connectivity and both higher-order cognition and general psychopathology. Together, our findings reveal a hierarchical axis in the development of structural connectivity across the human connectome.

Keywords

Adolescence, Development, Diffusion MRI, Structural Connectivity, Sensorimotor-association Axis.

Introduction

Myelinated axons play a central role in neuronal signal conduction, with large bundles of parallel axons comprising macroscopic white matter tracts(Sampaio-Baptista and Johansen-Berg, 2017). These white matter tracts interconnect the human cerebral cortex, forming a complex network of structural connectivity known as the connectome(Sporns et al., 2005). Both animal studies and human neuroimaging have provided evidence that the white matter structural connectivity is refined throughout childhood and adolescence(Baum et al., 2017; Bethlehem et al., 2022; de Faria et al., 2021; Lebel et al., 2019; Riccomagno and Kolodkin, 2015). The developmental refinement of structural connectivity results from a combination of microscale changes, such as myelination and alterations of axon diameter, which occur during varying developmental periods for different white matter tracts (de Faria *et al.*, 2021; Riccomagno and Kolodkin, 2015; Sampaio-Baptista and Johansen-Berg, 2017). Elucidating how developmental changes in structural connectivity strength spatially and temporally progress across the human connectome can reveal how the brain prioritizes refining structural connectivity at specific developmental stages and how heterogeneity in connection-specific developmental refinement impacts cognitive development. This understanding provides insight into how structural connectivity is susceptible to influences such as exposure to psychopathology and interventions at distinct developmental periods.

Animal studies have revealed that activity- and experience-dependent plasticity in myelination and axonal remodeling are driving factors in the developmental maturation of white matter structural connectivity in youth(Chereau et al., 2017; de Faria *et al.*, 2021; Fields, 2015; Riccomagno and Kolodkin, 2015). During early development, sensorimotor connections experience high levels of neural activity transmission due to the rapid acquisition of motor skills and exposure to new sensory inputs. This heightened activity leads to increased expression of growth factors such as brain-derived neurotrophic factor (BDNF) and neuregulin-1, which subsequently promote axonal remodeling, dendritic arborization, and myelination in sensorimotor pathways(Fields, 2015). In contrast, association connections undergo a more prolonged period of development into young adulthood, which may be attributed to continued cognitive development and the capacity for more varied experiences to engage the neural circuits underlying higher-order cognitive functions(Sydnor et al., 2021). However, beyond this coarse division between sensorimotor and association connections, there is marked spatiotemporal variability in the developmental patterns of structural connectivity, particularly in the human connectome, which remains under-characterized. Moreover, it remains unclear how the spatial heterogeneity in connection-specific developmental refinement across the human connectome associates with cognitive and psychopathological outcomes during youth.

Recent studies support a unifying developmental framework that the asynchronous cortical maturation progresses along the sensorimotor-association (S-A) axis: a hierarchical axis of human brain organization that spans continuously from primary sensorimotor to transmodal association cortices(Sydnor et al., 2021). This framework posits that during childhood and adolescence, sensorimotor cortices tend to mature earliest, while association cortices exhibit a protracted

developmental trajectory, with a continuous spectrum of maturational patterns observed between them. Recent empirical data indicate that the development of regional intracortical myelin(Baum et al., 2022), intrinsic activity amplitude(Sydnor et al., 2023), and functional connectivity((Luo et al., 2024; Pines et al., 2022) unfolds along the S-A axis across the cortex during youth. In this study, we aimed to test the hypothesis that the developmental maturation of white matter structural connectivity is spatiotemporally organized along the S-A axis of the human connectome, with a spectrum of varying developmental trajectories with sensorimotor-sensorimotor and association-association connections as two ends. As brain development in youth is linked to both higher-order cognition and a variety of mental disorders(Baum et al., 2017; Insel, 2014a; Sydnor et al., 2021), we also hypothesized that the spatiotemporal heterogeneity of structural connectivity development would have implications in both cognitions and psychopathology. The asynchronous maturation of white matter structural connectivity can be studied non-invasively with diffusion MRI (dMRI) tractography, which reconstructs the connectivity of white matter tracts by tracing the diffusion of water molecules in the human brain(Le Bihan, 2003; Thiebaut de Schotten and Forkel, 2022). While challenged by limitations in resolving crossing fibers, white matter tracts derived from dMRI have been shown to be a valid approximation when compared to both classical dissections of post-mortem brain tissues and in vivo animal tract-tracing, particularly for large-scale anatomical pathways(Girard et al., 2020; Lawes et al., 2008; van den Heuvel et al., 2015; Yendiki et al., 2022).

Here, we employed dMRI to measure large-scale white matter connectivity to evaluate our hypothesis that the developmental program governing structural connectivity refinement is hierarchically organized along an S-A axis of the human connectome during youth. Based on the canonical S-A cortical axis(Sydnor et al., 2021), we first defined an S-A connectional axis that continuously progresses from sensorimotor-sensorimotor to association-association connections across the human connectome. We then quantified structural connectivity strength with the number of white matter streamlines, which were reconstructed with probabilistic fiber tractography, connecting pairs of large-scale cortical systems. We hypothesized that the development of structural connectivity strength would be primarily characterized by heterochronous increases that align with the S-A connectional axis. Moreover, we hypothesized that the associations between structural connectivity strength and the individual differences in higher-order cognition would also be patterned on the human connectome along the S-A connectional axis. Human neuroimaging research has shown that increased segregation of structural connectivity in association networks is related to improved performance in higher-order cognitions(Baum et al., 2017). Therefore, we predicted that large-scale structural connectivity strength declined with higher cognitive performances. We particularly expected that the effect sizes of these associations increase along the S-A connectional axis, as association connections are more strongly related to the higher-order cognitions. Finally, given that mental disorders in youth are characterized by abnormal neurodevelopment(Insel, 2014a), we hypothesized significant associations between structural connectivity strength and psychopathological symptoms, and the strength of these associations would increase along the S-A connectional axis. Altogether, this work aims to contextualize the asynchronous maturation of structural connectome and connectome-linked cognitive and

psychiatric phenotypes in the framework of the S-A connectional axis.

Results

To delineate how age-related structural connectivity refinements spatiotemporally progress throughout the human connectome, we studied two independent datasets with both structural and diffusion MRI data. The first dataset consisted of 590 youths aged 8.1 to 21.9 years from the Lifespan Human Connectome Project in Development (HCP-D, **Figure 1A**, **Table S1**). The second data comprised children and adolescents from both baseline (N = 3,949, age 8.9–11.0 years) and two-year follow-up (N = 3,155, aged 10.6–13.8 years) within the longitudinal Adolescence Brain Cognitive Development (ABCD) study (**Figure 1B**, **Table S2**). See **Figure S1** and **Figure S2** for the detailed exclusion criteria of the two datasets. We constructed individuals' structural connectivity matrices using white matter tracts reconstructed from diffusion MRI data. Prior work has shown that diffusion MRI is reliable in detecting large-scale white matter tracts(Donahue et al., 2016; Girard *et al.*, 2020). Our study mainly focused on the large-scale white matter connectivity between cortical systems.

We partitioned the cerebral cortex into 12 large-scale distributed systems with approximately equal size according to regions' ranks in a priori defined regional sensorimotor-association (S-A) cortical axis map (**Figure 1C**), which was derived by averaging various cortical neurobiological properties(Sydnor et al., 2021). Cortical regions were ranked continuously along this axis, with sensorimotor cortices representing the lowest ranks and association cortices representing the highest. Consequently, our 12 large-scale cortical systems (**Figure 1D**) progressively spanned from primary sensorimotor to higher-order association cortices. After deriving this map of 12 cortical systems based on S-A axis rankings, we reconstructed individuals' whole-brain white matter tracts (**Figure 1E**) using probabilistic fiber tractography with multi-shell, multi-tissue constrained spherical deconvolution(Jeurissen et al., 2014). Anatomically constrained tractography (ACT)(Smith et al., 2012) and spherical deconvolution informed filtering of tractograms (SIFT)(Smith et al., 2015b) were applied to improve the biological accuracy of fiber reconstruction. We quantified the number of streamlines connecting each pair of the 12 cortical systems, scaled by their respective cortical volumes, resulting in a structural connectome of streamline counts for each participant (**Figure 1F**). The structural connectome was represented as a matrix of structural connectivity, organized into 12 rows and 12 columns based on the systems' ranking along the S-A cortical axis, progressing from the lower ranks of sensorimotor cortices to the highest ranks of association cortices.

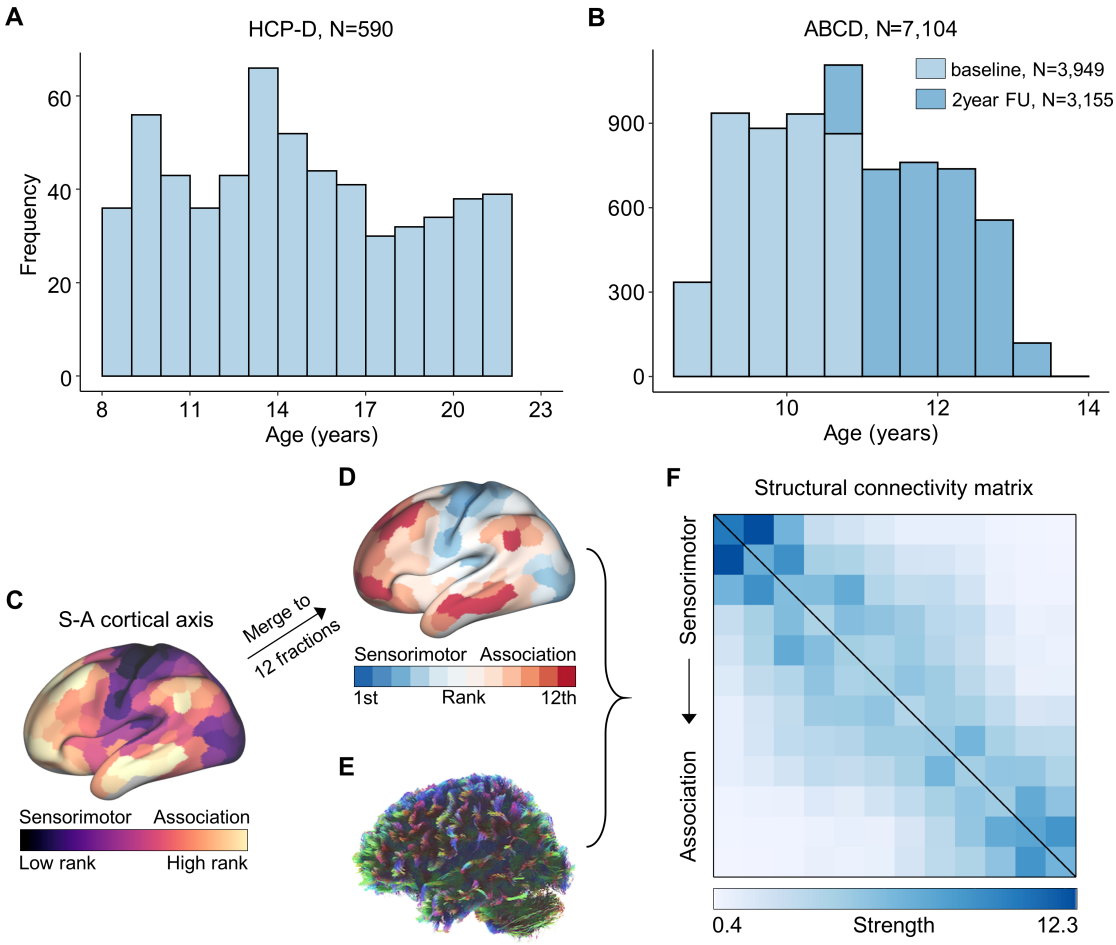

Figure 1. Distribution of participants' age and structural connectivity construction. **A,** Age distribution (8.1–21.9 years) of 590 participants from the HCP-D dataset. **B,** Age distribution of participants from baseline (N = 3,949, 8.9–11.0 years) and 2-year follow-up (N = 3,155, 10.6–13.8 years) within the ABCD study. Using the Schaefer-400 atlas based S-A cortical axis map(Sydnor et al., 2021) (**C**), a cortical atlas comprising 12 cortical systems (**D**) was generated. In the S-A cortical axis map, cortical regions were ranked continuously along this axis, ranging from the lowest rank in the sensorimotor cortices to the highest rank in the association cortices. The 12-system cortical atlas was constructed by approximately equally dividing the cortex into 12 fractions according to the regions' S-A cortical axis rank. For each scan, tractography was utilized to reconstruct the whole-brain white matter tracts with diffusion MRI dataset (**E**), and the large-scale white matter tracts connecting each pair of the 12 cortical systems were extracted and counted to generate the structural connectivity matrix (**F**). The connectivity matrix comprised 12 rows and 12 columns, with each element determined by the counts of white matter streamlines between every pair of systems, scaled by their respective cortical volumes. The matrix was arranged based on the average S-A axis cortical ranks of all regions within each system, from sensorimotor to association systems. HCP-D: the Lifespan Human Connectome Project Development; ABCD: the Adolescent Brain Cognitive Development; S-A: sensorimotor-association.

Developmental refinement of structural connectivity varies across the connectome

We initially investigated the refinement of structural connectivity from ages 8.1 to 21.9 years using the HCP-D dataset(Somerville et al., 2018). Using a generalized additive model (GAM), we found that 70 out of 78 connectivity edges exhibited a significant age-related developmental effect (false discovery rate-corrected P value, $P_{FDR} < 0.05$), while controlling for sex and head motion (**Figure 2A**). We assessed the magnitude of age effects using the variance explained by age (partial R^2) and determined their direction based on the sign of the average first derivative of the age smooth function. Our analysis revealed variations in age effects across all 78 connections, with the strongest effects observed in connections among primary sensorimotor systems, a relatively weaker effect in connections among higher-order association systems, and the lowest effect in connections between sensorimotor and association connections. By visualizing the developmental trajectories of each connection, we observed a continuous spectrum spanning connections that display an early steep increase followed by a plateau, to those exhibiting a late increase (**Figure 2B**).

To capture the variations in the shapes of developmental trajectories among structural connections, we calculated the average second derivative of age fits for each connection, allowing us to quantify the curvature shape of the curves. A negative second derivative indicates a developmental curve that is concave downward characterized by an earlier strengthening and plateaus, while a positive average second derivative signifies a curve that is concave upward with a temporally delayed developmental strengthening. We found that the second derivatives displayed a substantial heterogeneity across the connectome edges. Specifically, we observed positive second derivatives in connections among association systems and negative values in connections among sensorimotor systems (**Figure 2C**). Z-scoring the developmental fits for each connection to remove the effect size variance revealed a continuous spectrum ranging from the downward concavity observed in sensorimotor connections to the upward concavity observed in association connections (**Figure 2D**). As an illustration, the structural connectivity between primary sensorimotor systems demonstrated a significant increase in connection strength during childhood, reaching its peak during mid-adolescence (**Figure 2E**). In contrast, the structural connectivity between higher-order association systems is largely stable from childhood to early adolescence, followed by a significant and prolonged increase that accelerates notably into young adulthood (**Figure 2F**). By evaluating the rate of developmental change at each age window, we found that the declines were not significant for sensorimotor connection during late period (**Figure 2E**) or for association connection during early period (**Figure 2F**). Notably, with this analysis, we did not observe any periods of significant ($P_{FDR} < 0.05$) decrease among all 78 connections (**Figure S3**).

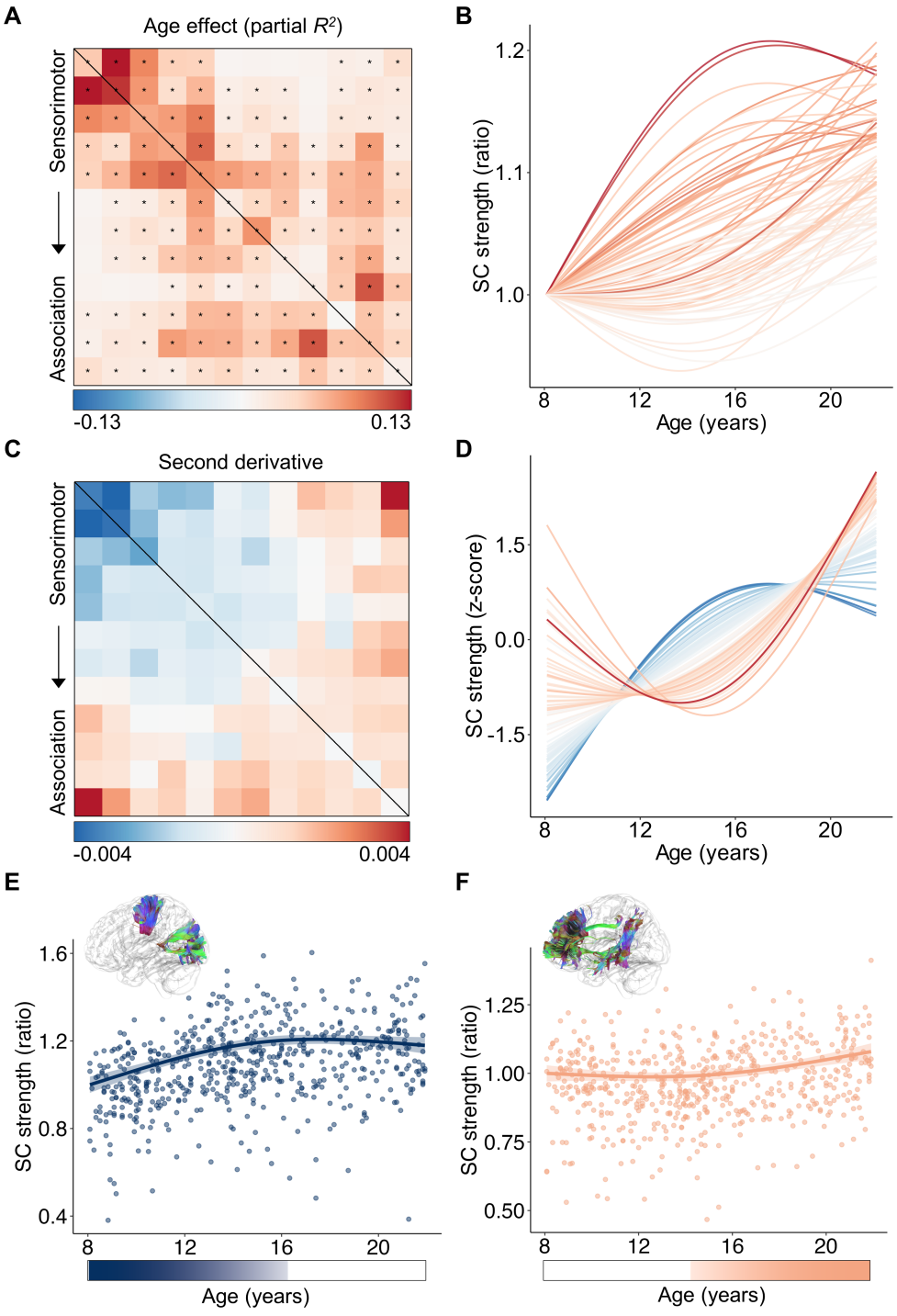

Figure 2. Developmental trajectories of large-scale structural connectivity spatiotemporally vary across the connectome in youth. A, The age effects (partial R^2) of structural connectivity strength were heterogeneously distributed across the connectome edges. Developmental effects were modeled using generalized additive models (GAMs). The black asterisks indicate statistically significant age effects ($P_{FDR} < 0.05$). **B**, The developmental trajectories of structural connectivity strength showed a continuous spectrum, ranging from an early increase to a later and prolonged

increase. The color of each curve was determined by the corresponding color in the effect size matrix shown in panel (**A**). **C**, The second-order derivatives of developmental curves in structural connectivity strength reveal a continuous spectrum of developmental trajectories across connectome edges. **D**, The z-scored developmental curves clearly illustrate that the curvature shapes of developmental trajectories continuously change along a spectrum from sensorimotor to association connections. The color of each curve was matched to the corresponding color in the matrix displayed in panel (**C**). **E**,**F**, Scatterplots depicting the developmental trajectories of structural connectivity between the 1st and 2nd systems involving primary visual and somatomotor cortices (**E**), and structural connectivity between the 11th and 12th systems involving higher-order frontal and temporal cortices (**F**). Data points in the scatter plots represent each participant (N = 590), the bold line indicates the best fit from a GAM, and the shaded envelope denotes the 95% confidence interval. The color bars below the two scatter plots depict the age windows wherein structural connectivity strength significantly changed, shaded by the rate of change. Diagrams of the two white matter tracts are situated above the scatter plots. SC: structural connectivity.

Developmental variability of structural connectivity aligns with the S-A connectional axis

Having demonstrated that the curvature shapes of the developmental profiles exhibit substantial heterogeneity across the connectome edges, particularly showing divergence between sensorimotor and association connections, we next evaluated whether variability in developmental trajectories of structural connectivity spatially aligns with the S-A axis. The S-A cortical axis serves as a unifying organizing principle encompassing diverse neurobiological properties, with a continuous progression observed along the axis from primary and unimodal sensorimotor to multimodal and transmodal association cortices(Sydnor et al., 2021). To compare our connectome edge-level developmental variability to the S-A axis, we converted the S-A cortical axis map into the S-A connectional axis. Specifically, we assigned a single S-A axis rank to each of the 78 connections by calculating the sum of the squared S-A cortical axis ranks for each pair of regions involved. This generated a continuous spectrum of S-A connectional axis ranks across the connectome, progressing from the lowest ranks in connections between sensorimotor systems to the highest ranks in connections between association systems (**Figure 3A**).

We next evaluated the relationship between the second derivative obtained from the age fits (**Figure 3B**, also see **Figure 2C**) and S-A connectional axis rank across all connections. Using Spearman's rank correlation, we identified a highly significant positive correlation between the second derivatives and S-A connectional axis ranks (rho = 0.79, $P < 0.001$, **Figure 3C**). This finding quantitatively demonstrates that connections among primary sensorimotor systems exhibited negative second derivatives in developmental trajectories, whereas connections between association networks displayed positive second derivatives. Furthermore, there is a continuous spectrum of second derivatives between these two extremes along the S-A connectional axis. To visually depict the progression of developmental trajectories of structural connectivity from the sensorimotor to the association end of the S-A connectional axis, we partitioned the axis into 10 decile bins and computed the average age fits across all connections within each bin. We then

visualized the z-scores of the average age fits. The continuous spectrum of developmental trajectories observed at the connectional level (**Figure 2D**) was mirrored by S-A connectional axis deciles (**Figure 3D**). Particularly, the connections located at the sensorimotor end of the S-A connectional axis displayed downward concave trajectories characterized by an early steep developmental increase followed by a plateau, while those situated at the association end exhibited upward concave trajectories with a late developmental increase.

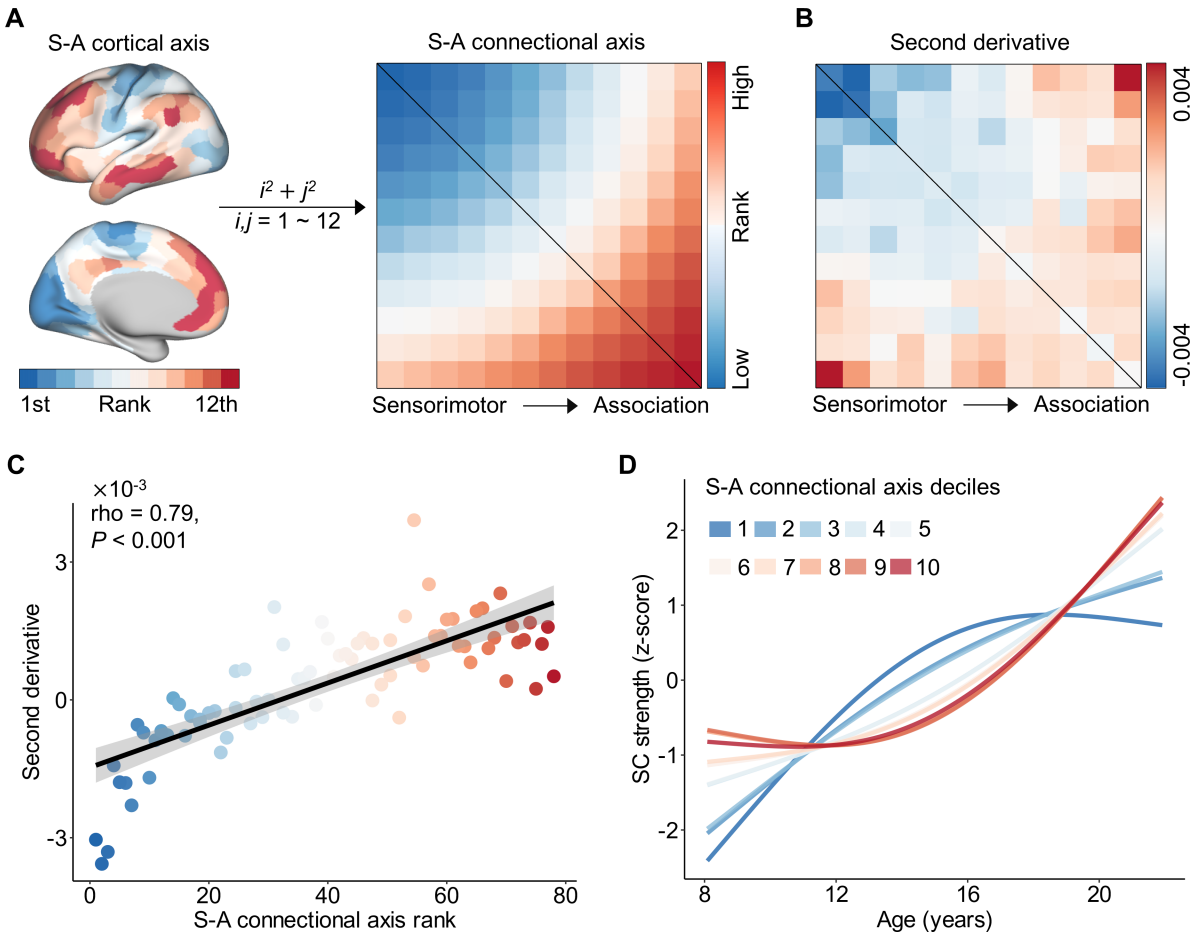

Figure 3. The heterogeneity of structural connectivity development across connectome aligns with the S-A connectional axis. A, The S-A connectional axis generated from the priori S-A cortical axis. A single connectional axis rank was assigned to each connection by summing the squares of pairwise systems' S-A cortical axis ranks. These connectional ranks were subsequently scaled into discrete values, ranging from 1 to 78. **B**, The second-order derivative of developmental trajectories in structural connectivity strength from **Figure 2C**. **C**, The second-order derivative is highly correlated (Spearman's rho = 0.79, $P < 0.001$) with the connectional axis rank across all structural connections. The color of all points was determined by the corresponding color in S-A connectional axis matrix. **D**, Averaging model fits depicting the developmental trajectory of structural connectivity are shown for deciles of the S-A connectional axis. To generate average

decile fits, the S-A connectional axis was divided into 10 bins each consisting of 7 or 8 large-scale structural connections, and age smooth functions were averaged across all connections in a bin. Subsequently, the average age fits were normalized with z-scores for visualization. The first decile (darkest blue) represents the sensorimotor pole of the S-A connectional axis, and the tenth decile (darkest red) represents the association pole of the axis. Maturation trajectories diverged most between the two connectional axis poles and varied continuously between them. SC: structural connectivity; S-A: sensorimotor-association.

Developmental alignment with S-A connectional axis shifts during youth

Having demonstrated that the developmental heterogeneity of structural connectivity across the connectome edges aligns with the S-A connectional axis, we further evaluated how this alignment evolves across the youth. For this analysis, the age range of 8.1 to 21.9 years was divided into 1,000 equally spaced intervals, within which the rate of development was assessed for each segment. Given the brevity of the interval, we assumed a linear developmental effect during this short period. We estimated the developmental rate in each segment as the first derivative to quantify the age-resolved developmental effect. By visualizing the rate of change for all structural connections across the S-A connectional axis from ages 8.1 to 21.9 years (**Figure 4A**), we observed a continuous spectrum of developmental patterns in connectivity change rates. This spectrum ranged from predominantly positive change rates during childhood and early adolescence in primary sensorimotor connections to association connections characterized by positive change rates during late adolescence and early adulthood. Notably, the negative change rates were not statistically significant for any connection (**Figure S3**).

We next evaluated how the alignment between the developmental change rates and S-A connectional axis ranks evolves from ages 8.1 to 21.9 years. To achieve this, we calculated the age-resolved spatial alignment between the connectome-wide change rates and S-A connectional axis for each of 1,000 age spaced intervals. This analysis revealed a continuous shift from a strong negative S-A axis alignment to a strong positive S-A axis alignment over development (**Figure 4B**). More specifically, there was a negative correlation that slowly increased to 0 before approximately 13 years, followed by a rapid increase in the correlation value until late adolescence around 18 years, ultimately reaching a stable period during young adulthood. Notably, a zero alignment was observed at the age of 15.5 years (95% confidence interval of 15.3 to 15.8 years), indicating a switch in the direction of alignment between developmental connectivity strengthening and the S-A connectional axis at this age point. This result suggests that the largest developmental increases occurred at the S-A axis sensorimotor pole and decline in strength along the S-A axis early in childhood (i.e., **Figure 4C**, left). During mid-adolescence, there was a clear switch in the patterning of effects such that the rate of developmental strengthening started to become stronger when moving from the sensorimotor to the association pole of the axis (i.e., **Figure 4C**, right). The matrices visualizing developmental change rates of all connections at ages 8.1, 15.5, and 21.9 years illustrate this transition (**Figure 4C**): from a pattern opposing the S-A connectional axis at 8.1 years old, to uniform developmental rates across all connections at 15.5

years old, and finally to a pattern closely aligned with the S-A connectional axis at 21.9 years old. The scatter plots depicting the correlation between change rates and connectional axis ranks confirmed this shift from negative to positive correlation during youth (**Figure 4D**).

As the age of 15.5 years suggests a transition point in the alignment with the S-A connectional axis, we expected to see a different spatial pattern of structural connectivity developmental effects between preceding and succeeding this critical age. We split all participants into two subsets, with 355 participants ages 8.1 to 15.5 years, and 235 participants ages 15.5 to 21.9 years old. We then re-evaluated the developmental effects of structural connectivity for the two subsets of participants separately using GAM. As with the full sample, the developmental effect was characterized by the variance explained by age (partial R^2) while controlling for sex and head motion. We observed that age effects were predominantly positive in sensorimotor connections and were negative in association connections from 8.1 to 15.5 years old (**Figure 4E, left**). A Spearman's rank correlation analysis revealed a negative association between age effects and S-A connectional axis ranks across all connections (Spearman's rho = -0.69, $P < 0.001$, **Figure 4E, right**). As expected, the reverse pattern emerged between the ages of 15.5 and 21.9 years: the age effects of sensorimotor connections were lower compared to those of association connections (**Figure 4F, left**), resulting in a significant positive correlation between age effects and S-A connectional axis ranks across all connections (Spearman's rho = 0.55, $P < 0.001$, **Figure 4F, right**). Overall, our findings suggest a rapid shift in the developmental program of structural connectivity refinement during mid-adolescence, with connections to association cortex exhibiting concerted strengthening after this shift.

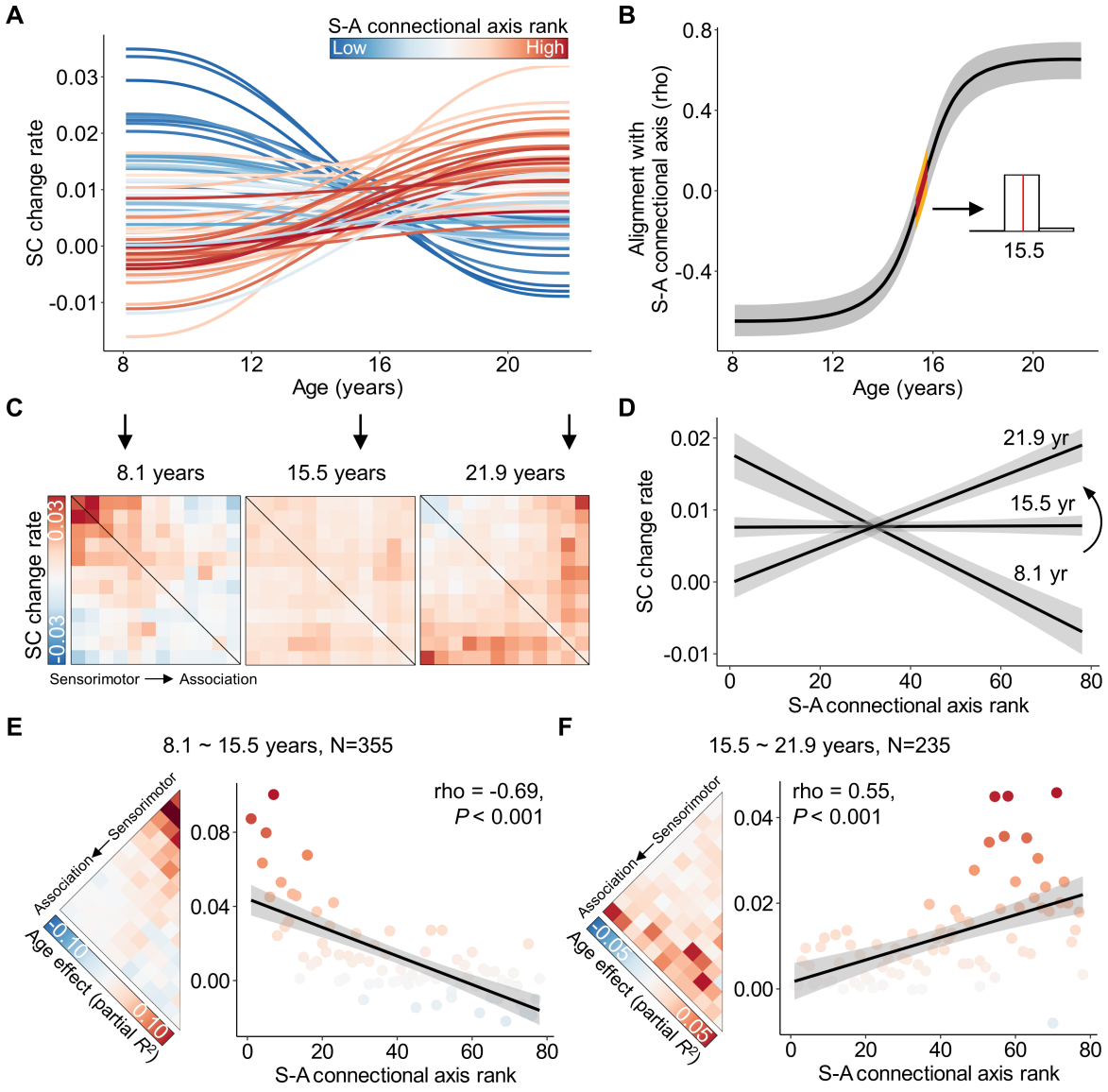

Figure 4. The spatial alignment between structural connectivity development and the S-A connectional axis shifts through youth. A, The rate (first derivative) of developmental changes of the large-scale structural connections from ages 8.1 to 21.9 years. Each line represents an edge, color-coded based on its rank in the S-A connectional axis. The change rates of connections at the sensorimotor pole of the S-A connectional axis decline from positive in childhood to slightly negative in young adulthood, while the connections at the association pole exhibited an opposite pattern. A continuous spectrum of the developmental patterns in structural connectivity change rates exists between the two S-A connectional axis poles. **B**, The alignment between the spatial patterning of structural connectivity development and S-A connectional axis evolves throughout youth. A spectrum ranging from the most pronounced negative association to zero-alignment around the age of 15.5 years, and then progressing to the most significant positive association is seen. To ensure the reliability of this alignment at different ages, we drew 1,000 samples from the posterior derivative of each connection's age smooth function and then proceeded to evaluate age-

resolved correlations between these derivatives and S-A connectional axis ranks for each sample. The black line on the plot represents the median correlation value across all samples, while the gray band indicates the 95% credible interval. Additionally, we identified the age of zero correlation between developmental changes and S-A connectional axis ranks for all 1,000 samples, with the corresponding 95% credible interval depicted by the yellow band. The distribution of ages with zero alignment from all samples is illustrated in the inset histogram (aged 15.3–15.8 years), revealing a median age of 15.5. **C**, The matrices of age-specific developmental change rates (first derivative) at ages 8.1, 15.5, and 21.9 years. **D**, Age-specific alignments (at ages 8.1, 15.5, and 22) between developmental effects and S-A connectional axis ranks across all edges. The plots depict a continuous transition from negative to positive alignment during development at 8.1, 15.5, and 21.9 years. **E**, **F**, Divergent developmental pattern of structural connectivity between younger and older youths. The age effects, estimated by partial R^2, exhibit a negative correlation with connectional axis ranks in younger youths (aged 8.1–15.5 years, Spearman's rho = -0.69, $P < 0.001$, (**E**)) and a positive correlation in the older youths (aged 15.5–21.9 years, Spearman's rho = 0.55, $P < 0.001$, (**F**)). The dot color is determined by the corresponding age effects in the matrix left side. Two edges with effect sizes of 0.18 and 0.16 were identified as outliers and removed in the scatter plot of panel (**E**). SC: structural connectivity; S-A: sensorimotor-association.

Independent longitudinal dataset confirmed developmental variability of structural connectivity along the S-A connectional axis

Using cross-sectional data from the HCP-D dataset, our results demonstrated alignment between the spatial variation of structural connectivity developmental trajectories and the S-A connectional axis during youth. We endeavored to replicate this finding using independent longitudinal data from the ABCD study(Casey et al., 2018). Our analysis included both baseline and two-year follow-up data, spanning ages from 8.9 to 13.8 years (**Figure 1B**). Given that this age range did not reach 15.5 years, the critical age associated with a shift in the developmental alignments with S-A axis from negative to positive, we hypothesized that there would be a negative association between developmental effects and the S-A connectional axis ranks across connectome edges in this dataset, based on our earlier findings (**Figure 4E**). We also hypothesized that the spatial variation of developmental trajectories' shape, as quantified by the second derivatives, would align with the S-A connectional axis, consistent with our findings in HCP-D dataset (**Figure 3C**).

To test these hypotheses, we constructed the structural connectivity matrices based on our cortical atlas with 12 systems for each participant's scans in the ABCD dataset. Using generalized additive mixed models (GAMM) to model the longitudinal development of structural connectivity strength, we evaluated the age effect of each structural connection, while controlling for sex and head motion. Our analysis revealed a spectrum of age effects across the connectome, ranging from positive effect sizes in primary sensorimotor connections to negative effect sizes in higher-order association connections (**Figure 5A**). Spearman's rank correlation revealed a significant negative correlation between age effects and S-A connectional axis ranks across all structural connections

(rho = -0.69, $P < 0.001$, **Figure 5B**), suggesting the S-A connectional axis captured connectome-wide spatial heterogeneity of structural connectivity development. These results were consistent with what we observed in the HCP-D dataset at younger ages (**Figure 4E**).

Furthermore, the average second derivatives of developmental trajectories demonstrate a positive correlation with the S-A connectional axis ranks across all connections (rho = 0.81, $P < 0.001$, **Figure 5C, D**), which also aligns with the findings in HCP-D (**Figure 3C**). Next, we replicated the evolution of the age-resolved change rate in structural connectivity strength. We also observed that the correlation between the age-resolved change rate and the S-A connectional axis ranks across all connections increased from a highly negative value to a near-zero correlation from 8.9 to 13.8 years old (**Figure 5E**). This continuous transition was further confirmed by fitting correlation plots between change rates and S-A connectional axis ranks at 8.9 and 13.8 years, respectively (**Figure 5F**). These findings align with the observed pattern in the HCP-D dataset.

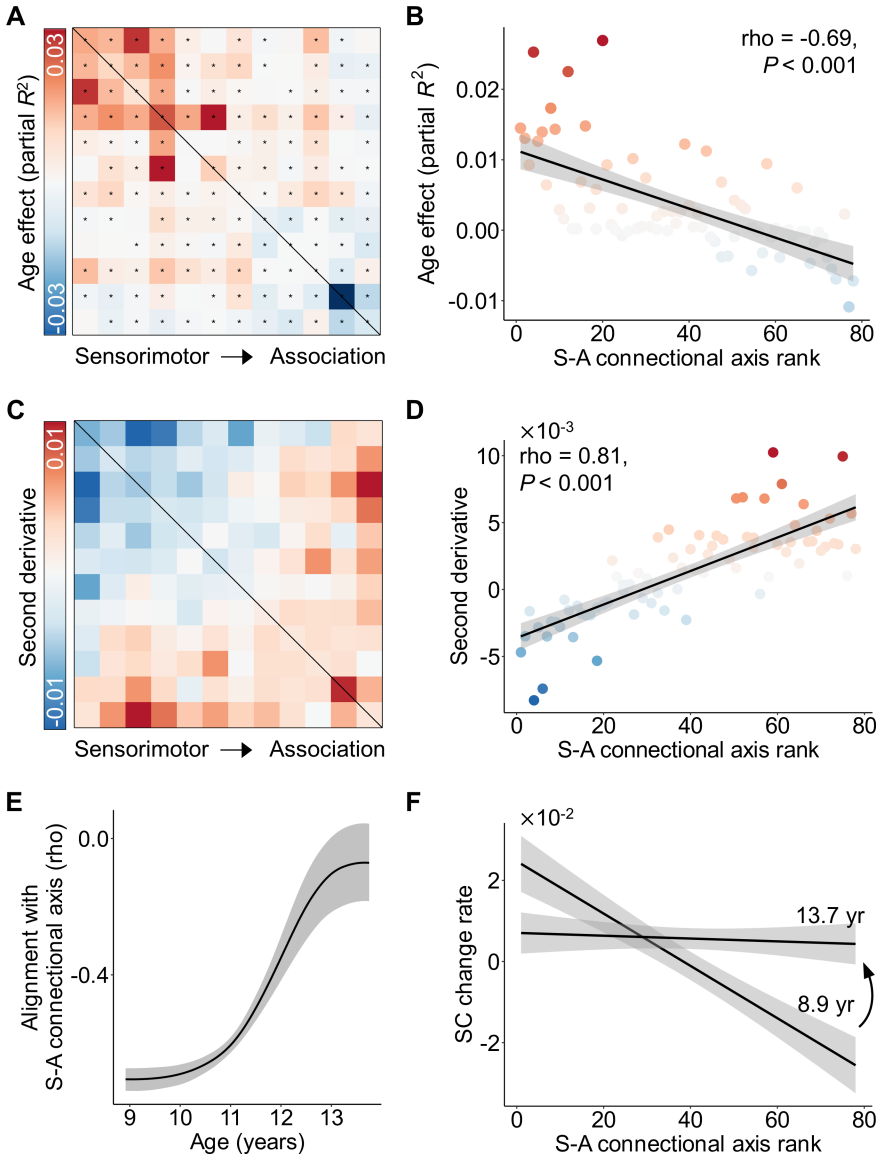

Figure 5. Longitudinal development of structural connectivity unfolds along the S-A connectional axis in an independent youth sample. A, Age effects (partial R^2) of longitudinal structural connectivity development through ages 8.9 to 13.8 years in the ABCD children. The black asterisks indicate statistically significant age effects ($P_{FDR} < 0.05$). **B**, The age effects were negatively correlated with the S-A connectional axis rank across all structural connections (Spearman's rho = -0.69, $P < 0.001$). The dots represent connections and were colored by the corresponding color in the age effect matrix of the panel (**A**). One edge with an effect size of -0.04 was identified as an outlier and removed in the correlation analysis. **C**, The second-order derivative of structural connectivity developmental trajectories. **D**, The second-order derivative was highly correlated with the connectional axis rank across all structural connections (Spearman's rho = 0.81, $P < 0.001$). The color of all dots was determined by the corresponding color in the second derivative matrix of the panel (**C**). **E**, The spatial variation of structural connectivity developmental changes negatively align with S-A connectional axis and the magnitude of this negative alignment

declined. **F**, Age-specific fitting of the relationship between change rates of connectivity strength and S-A connectional axis ranks shows the strongest negative correlation at the youngest age (i.e., 8.9 years) and the weakest association at mid-adolescence (i.e., 13.8 years). SC: structural connectivity; S-A: sensorimotor-association.

Cognitive associations of structural connectivity vary along the S-A connectional axis in adolescence

Previous studies have shown that structural connectivity strength associates with individual differences in higher-order cognition during youth(Baum et al., 2017; Lebel *et al.*, 2019), however, the connectome-wide spatiotemporal variability of this association remains uncharacterized. Here, we proceeded to evaluate whether the associations between structural connectivity strength and cognitive performance differ along the S-A connectional axis on the human connectome. To do this, we employed the datasets from both the HCP-D and ABCD study and selected the composite score of fluid cognition to assess individuals' performance in higher-order cognitive functions(Weintraub et al., 2013). The composite score was obtained by averaging the normalized scores from several cognitive tasks, including flanker inhibition, dimensional change card sort (flexibility), list sorting working memory, picture sequence episodic memory, and pattern comparison processing speed (**Figure 6A**).

We employed GAM analyses to model the linear association between fluid cognition and structural connectivity strength while controlling for the spline of age, sex, and head motion as covariates, for both the HCP-D and ABCD datasets. As the 2-year follow-up data from the ABCD study did not include flexibility and working memory behaviors, our analysis focused solely on the baseline data from individuals aged 8.9 to 11.0 years for ABCD. We did not observe significant cognitive effects in the HCP-D dataset, which may be due to the limited sample size. However, in the ABCD dataset, we found that 72 out of 78 structural connections exhibited a significant association between structural connectivity strength and individual differences in higher-order cognition during childhood ($P_{FDR} < 0.05$, **Figure 6B**). Notably, all significant correlations were negative, indicating that weaker structural connectivity between the large-scale cortical systems was linked to stronger performance in higher-order cognition. Furthermore, the effect sizes continuously increased along an axis from edges connected to the sensorimotor systems to those connected to the association systems. Using Spearman's rank correlation, we found that the cognitive effects of structural connectivity were negatively associated with the S-A connectional axis ranks across all connections with marginal significance (**Figure 6C**). This quantitative result confirmed that sensorimotor connections at the lower end of the S-A connectional axis exhibited weaker cognitive relationships, while association connections at the upper end of the axis showed stronger cognitive effects. Exemplifying this pattern, there was a decline in fluid cognitive scores associated with stronger structural connectivity strength for the connection between the 5th and 6th cortical systems (S-A connectional axis rank = 23), between the 2nd and 11th systems (S-A connectional axis rank = 48), as well as between the 10th and 11th systems (S-A connectional axis rank = 73) (**Figure 6D**).

We next evaluated if developmental trajectories of structural connectivity strength differ for youth with different levels of cognitive performance. While we only have baseline cognitive data, we included both baseline and two-year follow-up dMRI data to characterize the structural connectivity development as above. We modeled age-dependent changes in structural connectivity strength as a function of cognitive scores, while controlling for age, sex, and head motion. Using GAMs with an age by cognition interaction, we predicted the developmental trajectories of structural connectivity strength for low and high levels of cognitive performance respectively. To define these levels, we used the 10th percentile of baseline cognitive performance for the low level, and the 90th percentile for the high level. We observed that children with poorer cognitive performance exhibited a prominent and prolonged increase in connectivity strength of sensorimotor connections (deciles 1 and 3), along with an earlier inflection point and an earlier increase in the strength of association connections (deciles 8 and 10), during the age range of 8.9 to 13.8 years old (**Figure 6E**). These result suggests that S-A connectional axis capture the spatial variation of relationship between structural connectivity strength and cognitive performance, and the connectivity strength developmental trajectories differ between populations with different levels of cognitive performance during childhood and adolescence.

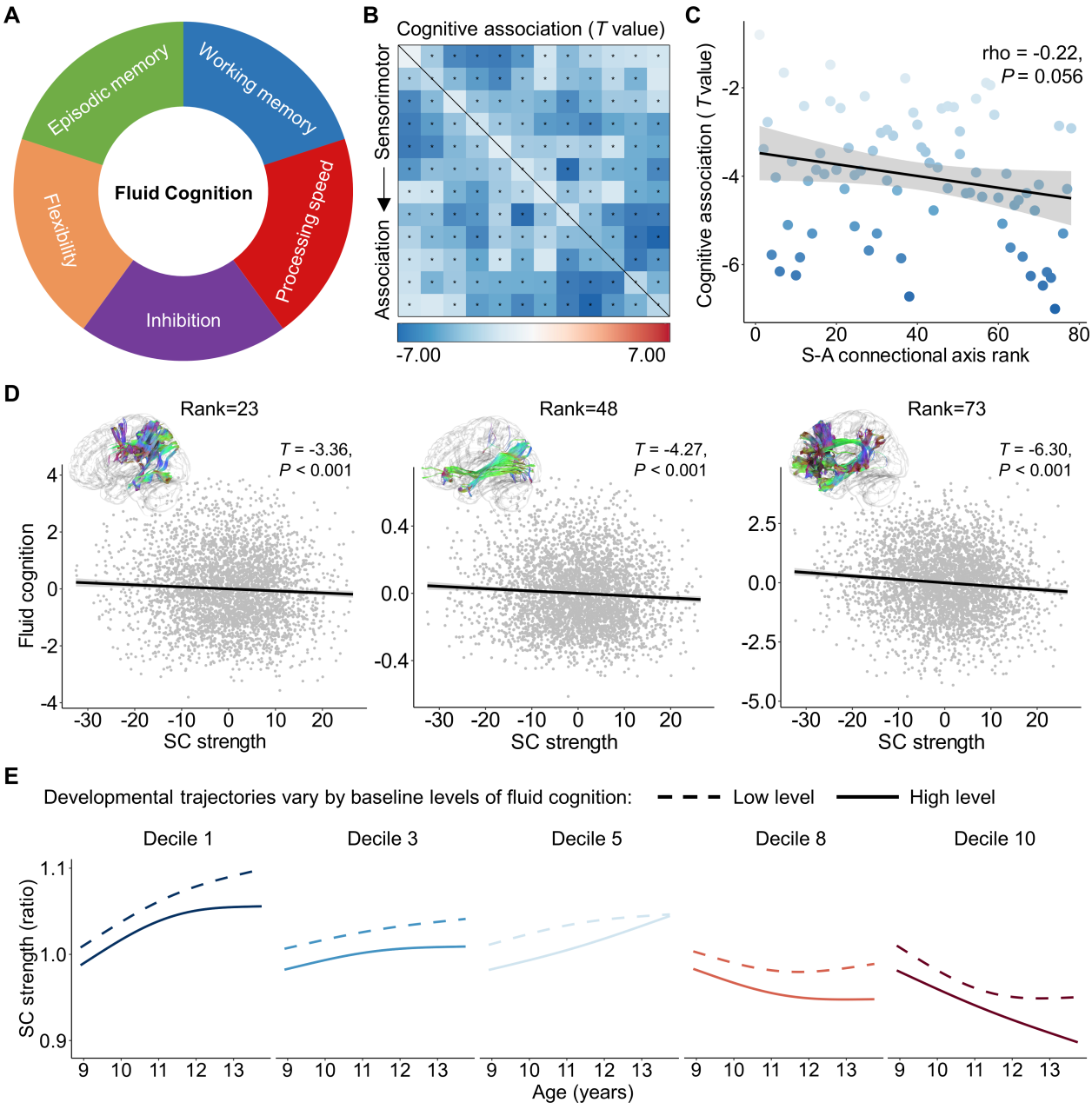

Figure 6. The spatial variation of the association between structural connectivity strength and higher-order cognition aligns with the S-A connectional axis. **A**, Fluid cognition is a composite score of flanker inhibition, dimensional change card sort (flexibility), list sorting working memory, picture sequence episodic memory, and pattern comparison processing speed. **B**, Structural connectivity strength is associated with the individual differences in fluid cognition across 3,871 children within the ABCD baseline dataset. The black asterisks indicate statistically significant associations ($P_{FDR} < 0.05$). **C**, The effect sizes of the association between connectivity strength and fluid cognition negatively related (Spearman's rho = -0.22, $P = 0.056$) to the S-A connectional axis ranks across all connections. **D**, Scatterplots of the association between structural connectivity strength and fluid cognitive performance for the three connectome edges with an S-

A connectional axis rank of 23, 48, and 73, respectively. The x and y axes represent the residuals of structural strength and fluid cognitive performance after regressing out age, sex and head motion. Data points in the scatter plots represent each participant, the bold line indicates the best fit from linear models, and the shaded envelope denotes the 95% confidence interval. **E**, The developmental trajectories of structural connectivity strength are displayed for populations with low (the 10th percentile) and high (the 90th percentile) cognitive performance for five deciles of the S-A connectional axis. SC: structural connectivity; S-A: sensorimotor-association.

Associations between structural connectivity and general psychopathology vary along the S-A connectional axis in adolescence

Psychiatric disorders have been increasingly conceptualized as neurodevelopmental disorders that involve altered maturation of higher-order association cortices that support complex cognition(Insel, 2014a; Sydnor et al., 2021). Therefore, we investigate whether there were associations between structural connectivity strength and psychiatric symptomatology during youth, and whether associations were strongest for association-association connections. Substantial comorbidity is prevalent across psychiatric disorders and recent studies have proposed that such comorbidity can be captured by a general psychopathology factor, also referred to as '*p*-factor'. An individual with a higher *p*-factor is susceptible to a shared vulnerability to a broad range of transdiagnostic psychiatric symptoms. We investigated whether the S-A connectional axis captures the spatial variability of relationships between structural connectivity strength and individual differences in this general psychopathology factor.

To do this, we employed the structural connectivity and psychiatric symptoms assessed using the Child Behavior Checklist (CBCL) from both the baseline and two-year follow-up data from the ABCD study. Based on a previously defined structure(Moore et al., 2020), we calculated the general psychopathology factor ('*p*-factor') for each participant with 66 items from the CBCL data, using confirmatory bi-factor analysis (**Figure 7A**). The general psychopathology factor summarizes the shared vulnerability across all the 66 CBCL clinical items. We next evaluated the linear association between the structural connectivity strength and general psychopathology factor using GAMMs that included per-participant random intercepts, while controlling for age, sex, and head motion. We found that the associations were mostly positive across all connections and a total of 11 connections showing statistically significant associations ($P_{FDR} < 0.05$), suggesting that a higher *p*-factor was related to greater structural connectivity strength (**Figure 7B**). Moreover, we observed that effect sizes increased along a continuum from the edges connected with sensorimotor systems to those connected within association systems. Using Spearman's rank correlation, we observed a positive relationship between the *p*-factor effects of structural connectivity strength and the S-A connectional axis ranks across all connections (rho = 0.50, $P < 0.001$, **Figure 7C**). This result indicates that, as with both developmental and cognitive effects, associations between structural connectivity strength and the general psychopathology factor were also patterned on the connectome along the canonical S-A axis. Exemplar scatter plots show how the general psychopathology factor positively associates with structural connectivity strength for the

connection between the 6th and 8th systems (S-A connectional axis rank = 38), between the 4th and 12th cortical systems (S-A connectional axis rank = 61), as well as between the 10th and 11th systems (S-A connectional axis rank = 73) (**Figure 7D**).

We next examined whether structural connectivity developmental trajectories are predicted to differ in individuals with different levels of psychiatric symptomatology. To do so, we modeled age-dependent changes in structural connectivity strength as a function of the *p*-factor, while controlling for sex and head motion. Using the acquired model, we fitted structural connectivity strength for the participants with a low-level and high-level of *p*-factor, respectively. We used the 10th percentile of *p*-factor to represent the participants with no or mild psychiatric symptoms, and the 90th percentile for the participants with severe psychiatric symptoms. We found that the connectivity developmental trajectories primarily differed substantially between the two groups at the higher-order association connections, such as deciles 8 and 10 of the S-A connectional axis (**Figure 7E**), with a similar pattern observed in the previous part of the cognitive analysis. Particularly, we observed that the participants with a higher *p*-factor exhibited an earlier inflection point with stronger connectivity and started increasing earlier. These results suggest that psychopathology risk is differentially associated with structural connectivity across the S-A connectional axis, and also related to different developmental trajectories of structural connectivity between association regions during childhood and adolescence.

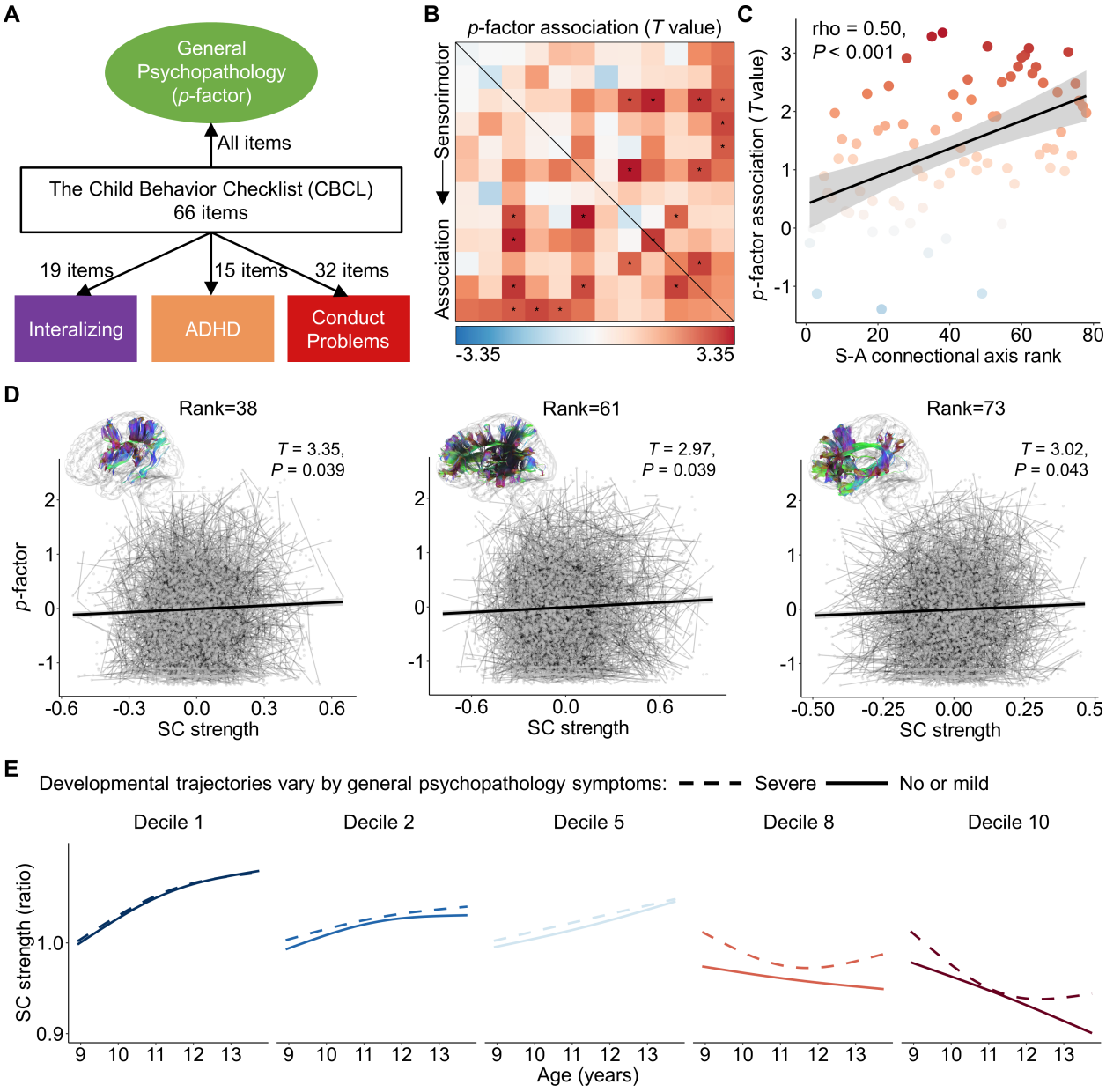

Figure 7. S-A connectional axis captures spatial variability of the association between structural connectivity strength and general psychopathology factor. A, A confirmatory bi-factor analysis revealed four independent psychopathology dimensions derived from the 66 clinical items assessed by the Child Behavior Checklist (CBCL). The general psychopathology factor, also referred to as '*p*-factor', captures shared vulnerability to a broad range of psychiatric symptoms. **B**, Linear associations between structural connectivity strength and individual differences in the general psychopathology factor. The black asterisks indicate statistically significant associations ($P_{FDR} < 0.05$). **C**, The effect sizes of the association between structural connectivity strength and *p*-factor positively associated with S-A connectional axis ranks across all the connections (Spearman's rho = -0.50, $P < 0.001$). **D**, Scatterplots of the association between structural connectivity strength and general psychopathology factor for the three connections with

a S-A connectional axis rank of 38, 61 and 73, respectively. The x and y axes represent the residuals of connectivity strength and *p*-factor after regressing out age, sex, and head motion. The pairs of points connected by thin lines represent two measurements for each participant from baseline and two-year follow-up. The bold line indicates the best fit from linear models and the shaded envelope denotes the 95% confidence interval. **E**, Developmental trajectories of structural connectivity are displayed for participants exhibiting severe psychopathological symptoms (at the 90th percentile of *p*-factor) and for those with no or mild symptoms (at the 10th percentile of *p*-factor) for five deciles of the S-A connectional axis. SC: structural connectivity; S-A: sensorimotor-association.

Sensitivity Analysis

We conducted several sensitivity analyses to evaluate the robustness of our findings to methodological variation including: 1) different resolutions of cortical parcellations with 7 systems (**Figure S4**) or 17 systems (**Figure S5**); 2) controlling for the effects of Euclidean distance between pairwise nodes (**Figure S6**); 3) additionally adding social-economic status (**Figure S7**) or intracranial volume (**Figure S8**) as covariates. Overall, our primary findings could be reproduced in all these analyses demonstrating the robustness of our results. See **Supplementary Text** for details of sensitivity analysis results.

Discussion

In this study, we leveraged non-invasive dMRI data from both cross-sectional and longitudinal developmental datasets to delineate how structural connectivity maturation spatiotemporally progresses across the human connectome during youth. We demonstrated that the structural connectivity developmental trajectories vary along a priori-defined S-A connectional axis. Particularly, we observed a continuous spectrum ranging from early age-related increases in connectivity strength between sensorimotor regions and post-adolescence increases in connectivity strength in association-association connections at the top end of the S-A axis. This developmental alignment with the S-A connectional axis evolved during youth, with a critical transition from negative to positive alignment occurring at approximately 15.5 years of age. Additionally, we found that the S-A connectional axis captures connectome-wide spatial variation in relationships between structural connectivity strength and both cognitive performance and transdiagnostic psychiatric symptomatology. Taken together, these results provide evidence of hierarchical development of structural connectivity along a macroscale connectional axis of the human connectome during youth.

White matter structural connectivity primarily consists of bundles of myelinated or unmyelinated axons connecting different brain regions(Sampaio-Baptista and Johansen-Berg, 2017). While evaluating white matter maturation during neurodevelopment can be challenging, dMRI offers a non-invasive approach to reconstruct macroscale bundles of white matter tracts in the human brain(Le Bihan, 2003). Using this technique, we have identified sustained increases in white matter structural connectivity strength throughout childhood, adolescence, and young adulthood. This finding is consistent with prior work showing a progressive increase in white matter volume throughout early life that peaks at 28.7 years of age(Bethlehem *et al.*, 2022). Moreover, we observed substantial heterogeneity in periods of increase across connectome edges. Connection strength began to increase before the earliest age studied (i.e., 8.1 years old) and ceased around 16 years old for unimodal sensorimotor-sensorimotor connections. In contrast, higher-order association-association connections began to strengthen around 14 years of age and exhibited rapid increases until the oldest age studied (i.e., 21.9 years old). The developmental trajectories of other sensorimotor-association connections displayed an intermediate pattern between these two extremes, forming a continuous spectrum of connectivity development across the human connectome.

These findings align with prior work showing that the development of white matter tracts exhibits asynchronous timing. Particularly, projection and commissural tracts have been shown to mature earlier (typically by late adolescence), while association tracts continue developing through late adolescence into early adulthood(Lebel and Beaulieu, 2011). Additionally, recent evidence has shown that the inferior and posterior parts of white matter tracts mature earlier than their superior and anterior counterparts(Bagautdinova et al., 2023). Expanding upon these coarse and qualitative comparisons of developmental timing among white matter tracts, our work provides a systematic description of the developmental sequence of white matter structural connectivity across the entire cortico-cortical connectome in humans. Notably, this sequence aligns with the

spatiotemporal progression of developmental changes in intrinsic cortical activity across the S-A cortical axis(Sydnor *et al.*, 2023), suggesting potential links between changes in the functional architecture of local cortical circuits and long-range cortico-cortical connectivity.

We further demonstrated that the connectome-wide spatial variation in structural connectivity development highly aligns with a pre-defined S-A connectional axis, which constitutes a continuum spanning from the sensorimotor-sensorimotor to association-association connections in the human connectome. A recent theoretical framework suggests that cortical neurodevelopmental plasticity progresses heterogeneously along the S-A cortical axis(Sydnor et al., 2021), and studies have shown that this axis captures the developmental chronology of regional neurobiological properties, including intracortical myelin(Baum *et al.*, 2022), intrinsic activity(Sydnor *et al.*, 2023), and functional connectivity strength((Luo et al., 2024; Pines *et al.*, 2022) in youth. Our results expand this framework to the structural connectome and provide initial evidence that the developmental sequence of structural connectivity conforms with the S-A axis throughout the human connectome. Furthermore, we identified a critical age period in mid-adolescence (15.5 years) at which time the alignment between spatial variation in structural connectivity development and the S-A connectional axis shifts from a negative to a positive association. Prior to this age period, the strength of sensorimotor connectivity primarily increases, while thereafter, the strength of association connectivity rapidly increases. Consistently, previous seminal work has shown that between the ages of 14 and 16, a putative functional marker of cortical plasticity peaks in association cortices and then starts to decline(Sydnor *et al.*, 2023). We speculate that the rapid developmental strengthening of association connectivity after the age of 15 could accelerate functional maturation in association regions and help to reduce regional variation in the patterning of spontaneously-generated activity across the cortex(Sydnor *et al.*, 2023).

Our study reveals a hierarchical pattern of white matter structural connectivity development, continuously progressing from sensorimotor-sensorimotor to association-association connections. This developmental pattern is likely shaped by a complex interplay of molecular, cellular, and activity-dependent processes. The myelination of axonal tracts has also been demonstrated to follow a chronologic sequence, wherein fibers belonging to specific functional systems mature simultaneously(de Faria *et al.*, 2021). Sensorimotor pathways undergo early myelination during development, whereas association pathways myelinate later during adolescence(de Faria *et al.*, 2021). This maturational sequence in myelination is driven by oligodendrocytes and regulated by various cellular and molecular mechanisms, such as transcription factors (Olig family), growth factors (BDNF, neuregulin-1), and hormones (T3)(Yu et al., 2023). The process of myelination is strongly influenced by experience- and activity-dependent plasticity mechanisms(Chereau *et al.*, 2017; Fields, 2015). For example, studies have demonstrated that signaling molecules regulated by action potential firing in axons can impact the development of myelinating glia(Fields, 2015). It is widely acknowledged that early development is primarily marked by new sensorimotor experience, whereas later developmental stages are characterized by prolonged exposure to increasingly complex cognitive and social experiences. Therefore, experience-driven and activity-

dependent myelin plasticity could be a primary mechanism underlying the maturational sequence of strengthening in white matter structural connectivity.

Our findings also revealed that structural connectivity strength was associated with higher-order cognitive performance, with the S-A connectional axis capturing the spatial variation in the strength of cognitive associations. Specifically, we first demonstrated that structural connectivity strength correlated with individual differences in higher-order cognition, assessed by a composite score comprising working memory, inhibition, flexibility, episodic memory, and pattern comparison speed(Akshoomoff et al., 2013). Notably, nearly all connections exhibited a negative relationship, indicating that weaker structural connectivity between large-scale cortical systems is related to stronger cognitive performance. This finding aligns with prior literature suggesting that enhanced segregation of brain network modules is linked to improved executive function(Baum et al., 2017; Finc et al., 2020; Keller et al., 2023b; Pines *et al.*, 2022). Furthermore, our findings revealed that the effect sizes of the negative association between connectivity strength and cognition progressively increase along the connectional axis, from sensorimotor-sensorimotor to association-association connections. This result is consistent with previous accounts emphasizing the primary role of association connections, rather than sensorimotor connections, in higher-order cognitions(Baum et al., 2017; Keller et al., 2023a; Menon and D'Esposito, 2022; Shen et al., 2020). Our study also contributes additional insight by demonstrating that the magnitudes of this relationship continuously change across the landscape of the human connectome. Importantly, we observed that populations with different levels of cognitive performance displayed distinct developmental trajectories in structural connectivity. Particularly, participants with higher cognitive abilities exhibited a more pronounced decline and lower connectivity strength in association connections compared to those with lower cognitive abilities. This relationship may be mediated by the increased structural network segregation during development(Baum et al., 2017). Together, these findings support spatially varying cognitive impacts on the maturation of structural connectivity across the human connectome, with the most significant effects observed in association connections.

Finally, we observed that the association between structural connectivity and psychopathology was also patterned on the human connectome along the S-A connectional axis. Traditional psychiatric diagnostic systems, such as DSM-5(Edition, 2013), typically reply on categorical diagnoses that often fail to capture the spectrum characteristic of diseases characterized by varying severity and are marked by a high degree of comorbidity(Kotov et al., 2017). Accordingly, efforts such as the Research Domain Criteria have proposed dimensional models of psychopathology(Insel, 2014b; Kotov *et al.*, 2017). Related studies have identified a general psychopathology factor, also known as the '*p*-factor', which reflects shared vulnerability to a broad range of psychiatric symptoms(Caspi and Moffitt, 2018). Our findings indicated that nearly all structural connections exhibited a positive correlation between connectivity strength and the *p*-factor score. Furthermore, the magnitude of this relationship demonstrated a significantly positive correlation with the S-A connectional axis ranks across all connectome edges. These results suggested that participants with higher *p*-factor scores tended to exhibit stronger structural

connectivity strength for association connections, which potentially reduced the network modules segregation. These results align with previous literature indicating that the loss of segregation between higher-order association functional networks, such as the default mode and fronto-parietal networks, represents a common deficit across psychopathology dimensions(Xia et al., 2018). We also observed that the levels of the general psychopathology factor influence the developmental trajectories in association connections. Populations with a severer *p*-factor exhibited earlier connectivity maturation and stronger connectivity strength. This psychopathological effect on structural connectivity development demonstrates a distinctly opposite pattern compared to the cognitive effects, suggesting that altered structural connectivity development associated with worse cognition or greater psychopathology may operate through similar mechanisms.

Several potential limitations of the present study should be noted. First, precisely reconstructing individuals' white matter structural connectivity is challenging; prior studies have demonstrated that dMRI-based fiber tractography may encounter false positives and negatives(Maier-Hein et al., 2017). In this study, we used state-of-the-art probabilistic fiber tractography with multi-shell, multi-tissue constrained spherical deconvolution(Jeurissen et al., 2014). Additionally, we applied anatomically constrained tractography(Smith *et al.*, 2012) and spherical deconvolution-informed filtering of tractograms(Smith et al., 2015a) to improve biological accuracy. Consistency-based thresholding was also employed to reduce the influence of false-positive connections(Baum et al., 2020). Moreover, previous studies have consistently shown the reliability of dMRI-based tracing of large-scale white matter bundles(Donahue *et al.*, 2016; Girard *et al.*, 2020). Our study focused on analyzing large-scale structural connectivity between cortical systems rather than delving into finer between-regional connectivity. This approach ensured the reliability of our structural connectivity analysis. While large-scale network analysis has been widely used in functional networks in recent years(Cui et al., 2020; Gordon et al., 2017; Wang et al., 2015; Yeo et al., 2011), it has been seldomly considered in structural networks. Our study thus offers a significant methodological contribution, potentially inspiring a shift towards a research paradigm emphasizing large-scale structural connectivity over finer between-regional structural connectivity with dMRI.

Second, both the cognitive and psychopathological measures were composite scores derived from aggregating a set of interrelated variables, precluding inference about specific associations between structural connectivity and individual traits. Future investigations should aim to untangle the complex interplay between structural connectivity and specific cognitive or psychopathological components. Third, it's important to acknowledge that, although statistically significant, the effect sizes observed for both cognitive and psychopathological effects on structural connectivity were relatively small. However, prior work has consistently demonstrated that effect sizes tend to be inflated in small samples(Yarkoni, 2009), whereas larger samples provide a more accurate estimate of the true effect size. Notably, our findings revealed a strong relationship between effect size and S-A connectional ranks. Forth, our study primarily focused on understanding the developmental trajectories of structural connectivity between cortical systems. Future studies should extend this research to explore how the spatiotemporal variability

in structural connectivity development for subcortex and cerebellum, which play crucial roles in motor control, emotional processing, and cognitive functions(McFadyen et al., 2020; Sokolov et al., 2017).

Notwithstanding these limitations, our study provides compelling evidence that, throughout childhood and adolescence, developmental changes in structural connectivity and associations with cognitive and clinical factors follow a distinct pattern along the hierarchical S-A axis of the human connectome. These findings suggest the importance of considering connectome-wide spatial variation in connectivity maturation in the context of cognitive development and vulnerability to psychopathology. Insights into this spatial progression of structural connectivity maturation will facilitate discerning connection-specific sensitive time windows for experiential, environmental, and interventional influences. Given the importance of the S-A connectional axis in structural connectivity development, future studies could evaluate whether this organizing axis serves as a unifying developmental principle across multi-modal and multi-scale human and non-human primate connectomes.

Methods

Participants

Our study utilized two independent neurodevelopmental datasets. The first one was a cross-sectional dataset from the Lifespan Human Connectome Project in Development (HCP-D)(Somerville *et al.*, 2018). The HCP-D recruited typical developing participants aged 5 to 22 from four sites in the United States. We selected this dataset as the discovery dataset for developmental analyses, given its broad age range coverage. Initially, demographic, cognitive, and neuroimaging data from 653 participants were obtained from the NIMH Data Archive (NDA) Lifespan HCP-D release 2.0. From this initial pool, we excluded 20 participants due to incomplete diffusion magnetic resonance imaging (dMRI) data and 10 participants due to anatomical anomaly. Additionally, 18 participants under 8 years of age were excluded due to the small sample size and big head motion often reported in this age group (Greene et al., 2018). An additional 14 participants were excluded due to excessive head motion during dMRI scanning, identified by mean framewise displacement (FD) exceeding the mean plus three standard deviations (SD)(Pines et al., 2020). Ultimately, we included 590 participants (273 males, aged 8.1–21.9) from the HCP-D. Written informed consent and assent were obtained from participants over 18 years of age and parents of participants under 18 years by the WU-Minn HCP Consortium. All research procedures were approved by the institutional review boards at Washington University (IRB #201603135).

The second dataset was from the Adolescent Brain Cognitive Development (ABCD) study(Casey *et al.*, 2018). The ABCD study recruited and followed approximately 10,000 children aged 9 to 10 years across the United States. Up to the beginning of data analyses of the current study, the ABCD study had released neuroimaging data from the baseline and 2-year follow-up, covering ages 8.9 to 13.8 years. We selected this dataset as a replicated dataset for developmental analyses and also used it for cognitive analyses. Furthermore, given the ABCD dataset recruited participants with various psychiatric disorders, we performed psychopathological analyses using this dataset. We accessed neuroimaging data from the ABCD fast-tract portal in June 2022, and demographic, cognitive, and psychopathological measures from the ABCD release 5.1. The imaging data were acquired using scanners from SIEMENS, PHILIPS, or GE manufacturers. Our study exclusively utilized data from SIEMENS scanners, encompassing 5,803 scans from baseline and 4,547 scans from the 2-year follow-up, each including dMRI, associated field map, and T1-weighted imaging (T1WI). This decision aimed to mitigate bias from manufacturer variations and reduce computational costs. We selected the SIEMENS manufacturer because most data were collected by scanners from this manufactuer in the ABCD study. From these scans, we applied various exclusion criteria including: 1) not meeting the official imaging recommended inclusion criteria outlined in the release 4.0 notes (we adopted criteria from release 4.0 because release 5.1 was not available when the MRI processing was conducted.); 2) incomplete dMRI data or failure in unzip or format conversion process; 3) lack of parental fluency in English or Spanish; 4) lack of proficiency in English; 5) diagnosis of severe sensory, intellectual, medical or neurological issues; 6) prematurity or low birth weight (N = 2,350); 7) having contraindications to MRI scanning; 8) invalid data regarding age and sex; 9) failure in data processing; 10) excessive head

motion (mean FD > Mean + 3×SD). The criteria regarding demography and healthy conditions came from a prior study(Garavan et al., 2018). After applying these criteria, we included a total of 7,104 eligible scans for the subsequent analyses, comprising 3,949 from baseline (2,075 males, aged 8.9–11.0) and 3,155 from 2-year follow-up (1,701 males, aged 10.6–13.8). The study protocol was approved by the institutional review board of the University of California, San Diego (IRB# 160091). Before participation, parents or legal guardians provided written informed consent, and children provided verbal assent.

The flow charts of HCP-D and ABCD participant inclusion and exclusion are presented in **Figure S1, S2**. Additional demographic details for the included datasets are available in **Table S1, S2**.

Cognitive assessment

Both the HCP-D and ABCD studies assessed participants' cognitive abilities using NIH Toolbox Cognition Battery. This battery evaluates five fluid cognitive functions: flanker inhibitory control and attention, list sorting working memory, dimensional change card sort, picture sequence memory, and pattern comparison processing speed. Both datasets generated a composite score from these five cognitive measurements to reflect participants' fluid cognition (Akshoomoff *et al.*, 2013). Specifically, based on the NIH Toolbox national norms, raw scores from each task were converted into normally distributed standard scores, with a mean of 100 and a standard deviation of 15. These standardized scores were then averaged, and the resulting average score was re-standardized to acquire the composite score of fluid cognition (Weintraub *et al.*, 2013). We utilized the standard score without age correction in analyses of both the HCP-D and ABCD datasets.

Psychopathology assessment

Prior studies on dimensional psychopathology have identified a general psychopathology factor (also referred to as '*p*-factor'), which represents a shared vulnerability to broad psychiatric symptoms and accounts for the comorbidity across mental disorders(Caspi and Moffitt, 2018). The ABCD dataset constitutes a transdiagnostic dimensional sample covering a continuous spectrum, ranging from healthy participants to those at high risk for psychopathology, and participants diagnosed with at least one mental disorder. Therefore, we utilized this dataset for our psychopathological analyses. We utilized the score from the parent-report Child Behavior Checklist (CBCL) (Achenbach and Verhulst, 2009) as the psychopathological measurements for children from the ABCD study. The CBCL comprises 119 items describing emotional and behavioral symptoms in youth covering various Diagnostic and Statistical Manual of Mental Disorders (DSM) classifications. It has exhibited strong psychometric properties, making it a widely utilized tool in both clinical and research settings(Ebesutani et al., 2010).

Moore and colleagues established a bifactor model for the general psychopathology factor using CBCL measurements from the ABCD study, demonstrating adequate reliability and validity

of this *p*-factor(Moore *et al.*, 2020). This model utilized a total of 66 CBCL items and generated four independent psychopathology dimensions, including a general psychopathology factor (*p*-factor) and three specific factors: internalizing, attention deficit hyperactivity disorder (ADHD), and conduct problems (**Figure 7A**). Based on this model structure, we conducted confirmatory bifactor analyses on the entire sample from the ABCD study in release 5.1 (baseline N = 11,860; 1-year follow-up N = 11,201; 2-year follow-up N = 10,895; 3-year follow-up N = 10,095) using Mplus 8.3(Muthén and Muthén, 2017). We fitted the model using the entire sample to reduce bias due to subject selection or visit time on the item loadings. The model was stratified by sites and accounted for clusters of families, while constraining factor loadings to be equal across time points. The model exhibited acceptable fitting performance: the baseline model yielded a comparative fit index (CFI) of 0.96 (>0.90), a root mean square error of approximation (RMSEA) of 0.02 (<0.08), and a standardized root mean square residual (SRMR) of 0.06 (<0.08) referring to Hu and Bentler (1999) (Hu and Bentler, 1999).

MRI acquisition

MRI data in the HCP-D dataset were acquired using the same protocol on 3T SIEMENS Prisma scanners with a 32-channel head coil from four different acquisition sites. 3D T1-weighted imaging (T1WI) data with a resolution of 0.8 mm isotropic were scanned using Magnetization Prepared Rapid Gradient Echo (MPRAGE) sequence. Two sessions of dMRI with a voxel size of 1.5 mm isotropic were acquired. The sessions used opposite phase-encoding directions to facilitate the correction of distortion induced by the Echo Planar Imaging (EPI) sequence used in dMRI scanning. Each session includes 185 diffusion directions with two b-values of 1,500 and 3,000 s/mm^2, along with 14 b = 0 s/mm^2 images. Further details about MRI acquisition of the HCP-D have been described in the previous study(Harms et al., 2018).

The MRI data from the ABCD dataset were acquired using 3T SIEMENS scanners across 13 acquisition sites, with sequences harmonized across different sites. 3D T1WI data were acquired with a 1 mm isotropic resolution. The dMRI scans were acquired at a 1.7 mm isotropic resolution comprising 7 b = 0 s/mm^2 frames and 96 diffusion directions across 4 shells of b = 500 s/mm^2, 1,000 s/mm^2, 2,000 s/mm^2 and 3,000 s/mm^2. Additionally, fieldmap scans in the opposite phase-encoding direction to dMRI were acquired for EPI distortion correction. Further details regarding MRI acquisition for the ABCD study have been provided in previous studies(Casey *et al.*, 2018; Hagler et al., 2019).

MRI data processing

We acquired minimally processed T1WI from the HCP-D dataset and SIEMENS normalized T1WI from the ABCD dataset. Before our processing, the HCP-D T1WI underwent gradient distortion, anterior commissure-posterior commissure (ACPC) alignment, and readout distortion correction(Glasser et al., 2013). The ABCD T1WI underwent SIEMENS intensity normalization.

Initially, we applied the anatomical pipeline embedded in QSIPrep version 0.16.0 (https://qsiprep.readthedocs.io/)(Cieslak *et al.*, 2021) to the T1WI data from both datasets. QSIPrep is an integrative platform for preprocessing dMRI and structural imaging data and reconstructing white matter structural connectome (Cieslak et al., 2021) by incorporating tools from FSL(Jenkinson et al., 2012), DSI Studio (https://dsi-studio.labsolver.org/), DIPY(Garyfallidis et al., 2014), ANTs (https://stnava.github.io/ANTs/), and MRtrix3(Tournier et al., 2019). The anatomical pipeline conducted through ANTs included: 1) intensity non-uniformity correction; 2) removal of non-brain tissues; 3) normalization to the standard Montreal Neurological Institute (MNI) space. The skull-stripped T1WI in native space was used as the anatomical reference for the dMRI workflow. Normalization generated transformation matrices to register the atlas in MNI space to individual anatomical references. Next, the T1WI data were utilized to reconstruct surface and segment tissues through *FreeSurfer*(Fischl, 2012) (http://surfer.nmr.mgh.harvard.edu/). The surface pial and tissue segmentations would be used as anatomical constraints during the construction of the structural connectome. The HCP-D T1WI was processed based on the *FreeSurfer* workflow from the HCP processing pipelines(Glasser *et al.*, 2013), while the ABCD T1WI were processed using the recon-all pipeline through *FreeSurfer* version 7.1.1.

Raw dMRI data were acquired from both the HCP-D and ABCD datasets. We applied the dMRI pipeline embedded in the QSIPrep to the dMRI data from both datasets. The pipeline included: 1) aligning and concatenating runs of dMRI and associated field maps; 2) designating frames with a b-value less than 100 s/mm^2 as b = 0 volumes; 3) Marchenko-Pastur principal component analysis (MP-PCA) denoising through MRtrix3's *dwidenoise* function(Veraart et al., 2016); 4) Gibbs unringing through MRtrix3's *mrdegibbs* function(Kellner et al., 2016); 5) B1 bias correction through MRtrix3's *dwibiascorrect* function(Tustison et al., 2010); 6) head motion, distortion and eddy current corrections through FSL's eddy tool(Andersson et al., 2016); 7) coregistration to individual T1WI and realignment to ACPC orientation. During this process, distortion correction utilized b = 0 reference images with reversed phase encoding directions. Following the previous study(Power et al., 2014), the mean FD was calculated as the sum of the absolute values of the differentiated realignment estimates for each volume to estimate the head motion during the dMRI scans.

Reconstruction of structural connectome

For each scan, whole-brain probabilistic fiber tracking was conducted on the preprocessed dMRI using MRtrix3(Tournier *et al.*, 2019). Multi-sell multi-tissue constrained spherical deconvolution (CSD) was utilized to estimate the fiber orientation distribution (FOD) for each voxel through MRtrix3(Jeurissen *et al.*, 2014). We employed the anatomically constrained tractography (ACT) framework based on the hybrid surface and volume segmentation (HSVS) algorithm to enhance the biological accuracy of fiber reconstruction(Smith et al., 2020; Smith *et al.*, 2012). The surface pial and tissue segmentations constructed by *FreeSurfer* provided tissue anatomical information. Within the ACT framework, FOD-based tractography (iFOD2 algorithm)

was performed using the *tckgen* function(Tournier et al., 2010), generating 10 million streamlines with lengths ranging from 30 to 250 mm. To match the streamline densities with fiber densities estimated by CSD, the streamlines were filtered based on the spherical deconvolution of the diffusion signal using the *tcksift2* function(Smith *et al.*, 2015b). Next, we constructed structural connectivity matrices based on the Schaefer-400 atlas(Schaefer et al., 2018) using the *tck2connectome* function*(Hagmann et al., 2008)*. Due to the low diffusion signal-to-noise ratio reported(Concha et al., 2005), limbic regions were removed from the atlas, leaving 376 regions.

For the 376×376 connectomes across individuals, we applied a consistency-based thresholding method(Roberts et al., 2017) to mitigate the presence of spurious streamlines arising from probabilistic tractography. We computed the coefficient of variation (CV) for each edge across different scans from each dataset. Edge weights were determined by the streamline number scaled by pairwise nodes' volume. Following previous studies(Baum *et al.*, 2020; Ge et al., 2023), we generated a binary mask for each dataset to filter the spurious streamlines based on the threshold at the 75th percentile of CV.

Large-scale structural connectivity connectomes with larger-size nodes have demonstrated higher reproducibility and biological validity than connectomes with finer nodes(Cammoun et al., 2012; Chen et al., 2015; Sotiropoulos and Zalesky, 2019). Consequently, we computed large-scale structural connectivity matrices based on the 376×376 connectomes for the following statistical analyses. Previous studies on large-scale brain networks typically parcellated the cortex into 7 or 17 systems (Hermosillo et al., 2024; Power et al., 2011; Yeo *et al.*, 2011). Here, we selected a resolution of 12 cortical systems as the median value of this range. We also evaluated 7 or 17 systems in the sensitivity analyses to demonstrate the robustness of our findings. Particularly, we first ordered the 376 regions according to their position in the sensorimotor-association (S-A) cortical axis and then evenly partitioned the regions into 12 large-scale systems, each comprising 32 or 31 regions along the S-A cortical axis. The S-A cortical axis was derived from a multitude of cortical features to capture a cortical hierarchical gradient from lower-order unimodal areas to higher-order transmodal areas(Sydnor et al., 2021). Then, we computed the structural connectivity strength as the number of streamlines connecting two large-scale systems normalized by the volume of the paired systems. During this process, the spurious streamlines were removed based on the binary mask defined by the consistency threshold. Finally, we obtained a 12×12 large-scale structural connectome matrix containing 78 structural connections for each participant.

Development of structural connectivity strength in youth

We first evaluated the connectome-wide spatial variation in developmental trajectories of structural connectivity strength during youth. All statistical analyses were performed in R4.1.0. We fitted the developmental models for 78 large-scale structural connections in both the HCP-D and ABCD datasets. We utilized general additive models (GAMs) for the cross-sectional HCP-D dataset and general additive mixed models (GAMMs) for the longitudinal ABCD dataset to flexibly capture linear and non-linear age-related changes in structural connectivity strength. The

models were fitted using *mgcv* (Wood, 2017) and *gamm4* package(Wood, 2014). For each model, we set structural connectivity strength as the dependent variable, with age as a smooth term, and sex and mean FD as covariates, as shown in equation (1). Per-participant random intercepts were additionally included in the GAMMs. Smooth plate regression splines served as the basic function of the smooth term, and the restricted maximal likelihood approach was used to estimate smoothing parameters. Based on previous neurodevelopmental studies in youth(Baum *et al.*, 2022; Sydnor *et al.*, 2023), we selected the degree of freedom of the smooth function (k) as 3 to prevent overfitting. We additionally calculated the Akaike Information Criterion (AIC) for GAMs or GAMMs with k values ranging from 3 to 6 to assess the model fitting performance. Consistent with previous studies(Baum *et al.*, 2022; Sydnor *et al.*, 2023), the optimal fits for most models were observed at a k value of 3, confirming the suitability of $k = 3$.

$$\text{Structural connectivity strength} \sim s(\text{Age}, k = 3) + \text{Sex} + \text{Mean\_FD} \quad (1)$$

For each model, we evaluated the significance of the age effect by comparing the full model with a null model lacking the age term(Sydnor *et al.*, 2023) using parametric bootstrap testing via analysis of variance for GAMs and parametric bootstrap testing via the likelihood ratio test statistic for GAMMs with 1,000 simulations(Larsen and Luna, 2018). The model comparisons were supported by the *ecostats*(Warton, 2022) and *pbkrtest*(Halekoh and Højsgaard, 2014) packages. The P values were then adjusted using the false discovery rate (FDR) correction, with a significant threshold set at 0.05. We calculated the first derivative of the age smooth function for each model using the *gratia* package(Simpson, 2021) to assess the change rate of structural connectivity strength. The first derivatives were computed for 1,000 age points sampled at equal intervals within the age span. For derivatives at each age point, we computed the P values of the derivatives based on the 95% confidence interval and then adjusted the P values using the FDR method for 78 models. Age windows of significant development were identified when the first derivative had a $P_{FDR} < 0.05$. To assess the overall age effect, we calculated the partial R^2 between the full and null models and then assigned the sign based on the average first derivative of the smooth function(Sydnor *et al.*, 2023).

To visualize the developmental trajectory of structural connectivity strength for each connection, we predicted the model fits for 1,000 age points sampled at equal intervals within the age span. Covariates were set at the median for numerical variables and the mode for categorical variables. The structural connectivity strength was normalized by dividing the initial strength at the youngest age (HCP-D: 8.1 years; ABCD: 8.9 years) within the age span for visualization, termed as structural connectivity strength ratio. As shown in **Figure 2B**, we observed heterogeneity in the curvature of the developmental trajectories. To highlight this heterogeneity, we standardized the fits (z-scored) across the age span for each connection. The fiber bundle diagrams shown in **Figure 2E, F** were generated using DSI studio (https://dsi-studio.labsolver.org/).

As we observed heterogeneity in the curvature of developmental trajectories, we computed the average second derivatives of age via central finite differences to quantify this curvature. A positive value of the average second derivative indicates a concave upward trajectory, while a negative value indicates a concave downward trajectory. The greater the absolute value, the greater

the degree of curvature. Notably, there is significant variability in the average weights of structural connectivity strength across the connectome, ranging from 0.4 to 12.3. It is important to recognize that a higher first or second derivative does not necessarily imply a greater change rate or curvature of trajectory relative to the connection's initial strength. For instance, a connection starting with an initial strength of 0.5 and a first derivative of 0.1 will evolve faster than a connection with an initial strength of 5 and a first derivative of 0.2, relative to their starting points. To address this issue, we normalized the structural connectivity strength of each connection by its fitted value at the youngest age within the dataset's age span, resulting in a structural connectivity strength ratio relative to its initial strength. We then computed the first and second derivatives on the models with the structural connectivity strength ratio as the dependent variable. This normalization process does not alter the significance or magnitude of the age effect.

Definition of the S-A connectional axis

The S-A cortical axis provided a framework to characterize the heterochrony of postnatal regional neurodevelopment, suggesting that many cortical features progress along the S-A cortical axis during childhood and adolescence(Baum *et al.*, 2022; Luo et al., 2024; Sydnor *et al.*, 2023). Building upon this, we aimed to investigate whether the development of structural connectivity strength unfolds along the S-A axis in terms of connections. As shown in equation (2), we defined the element ($C_{i,j}$) between $node_i$ and $node_j$ in the matrix of the S-A connectional axis as the quadratic sum of the S-A cortical axis ranks of $node_i$ and $node_j$. Next, we computed the ranks of C as the S-A axis connectional rank.

$$C_{i,j} = Node\_rank_i^2 + Node\_rank_j^2 \quad (2)$$

This definition was based on the hypothesis that connections between high-order regions on the cortical axis occupy higher positions on the S-A connectional axis. We did not adopt $Node\_rank_i + Node\_rank_j$ because the simple addition resulted in many identical values in the ranking. In the context of a 12×12 large-scale connectome, the S-A connectional axis rank ranges from 1 to 78.

Developmental alignment with the S-A connectional axis

The main goal of this study is to determine if the spatial variation of structural connectivity development aligns with the S-A connectional axis. To achieve this, we utilized Spearman's rank correlation to evaluate the concordance and its significance between the S-A connectional axis rank and both 1) the magnitude and direction of developmental effects (partial R^2) and 2) the curvature of the developmental trajectories (average second derivative). To depict developmental trajectories along the S-A connectional axis continuously, we divided the S-A connectional axis into 10 decile bins, with each bin consisting of 7 or 8 large-scale structural connections. We then

calculated the average age within each bin and subsequently normalized these averages using z-scores (**Figure 3D**).

To comprehensively understand how alignment evolves across the youth, we performed an age-resolved analysis of the alignment between the developmental change rates of connectivity strength and the S-A connectional axis((Luo et al., 2024; Sydnor *et al.*, 2023). We calculated the first derivative to measure the developmental change rates. This approach enabled us to capture the evolving alignment of development with the S-A connectional axis across the targeted age span. To determine the correlation coefficient and 95% credible interval for these age-specific correlation values, we initially sampled 1,000 times from the specified multivariate normal distribution of the independent variables' coefficients for each connectional model. We then generated the posterior derivatives at 1,000 age points based on the posterior distribution of each connectional fitted model. Subsequently, we repeated the process of correlating the S-A connectional axis rank with 1,000 draws of the posterior derivative of the age smooth function at each of the 1,000 age points. The resultant distribution of correlation coefficients was utilized to determine the median and 95% credible interval of alignment at each age point. Additionally, we employed the sampling distribution of age-specific S-A connectional axis correlation values to identify the age at which the alignment flipped from negative to positive. This involved calculating the age at which the axis correlation was closest to zero across all 1,000 draws and reporting the median along with the 95% credible interval.

Based on the age-resolved analysis, we found a transition age of 15.5 years at which the alignment of developmental effects with the S-A connectional axis shifts from negative to positive in the HCP-D dataset. To test whether the overall structural connectivity developmental effects differ spatially before and after this critical age, we split all participants into two subsets (younger subset: N = 355, aged 8.1–15.5 years; older subset: N = 235, aged 15.5–21.9 years). We re-evaluated the developmental effects (partial R^2) of structural connectivity strength for the two subsets separately using GAMs with the same parameters as those used for the full sample. Then, we utilized Spearman's rank correlation analysis to test the alignment of the overall developmental effects (partial R^2) with the S-A connectional axis in the two subsets. Notably, we expected the replicated results from the ABCD dataset to be consistent with those found in the younger subset of the HCP-D because the age span of ABCD participants (8.9–13.8 years) was within the 8.1 to 15.5 years range.

Associations between structural connectivity strength and higher-order cognitions

Associations between fluid cognition and structural connectivity strength were examined within both the HCP-D and ABCD datasets. Due to the lack of measurements for working memory and flexibility, which are components of fluid cognition, in the 2-year follow-up data of the ABCD study, only baseline data from the ABCD dataset were included in the cognitive analyses. We employed GAMs to assess the relationships between the structural connectivity strength and fluid cognition ability for each connection, controlling for age, sex, and mean FD. The equation for

GAMs is shown below (equation (3)).

$$\text{Structural connectivity strength} \sim \text{Fluid cognition} + s(\text{Age}, k = 3) + \text{Sex} + \text{Mean\_FD} \quad (3)$$

The *T* values of the fluid cognition indicate the magnitude and direction of the association, and its significance was determined by comparing the full model with a null model lacking the cognition term. GAM comparisons utilized parametric bootstrap testing via analysis of variance with 1,000 simulations, facilitated by the *ecostats* package(Warton, 2022). The *P* values were then FDR corrected across all the 78 connections. We next evaluated the alignment of association magnitude and direction with the S-A connectional axis rank across all connections through Spearman's correlation analysis.

Furthermore, we depicted the developmental trajectories by different levels of fluid cognition to elucidate how structural connectivity strength evolved in individuals with varying cognition levels. To do this, we fitted an age-by-cognition interaction model for each connection controlling for sex, and mean FD (see equation (4) for the formula).

$$\text{Structural connectivity strength} \sim s(\text{Age}, \text{by} = \text{Fluid cognition}, k = 3) + s(\text{Age}, k = 3) + \text{Sex} + \text{Mean\_FD} \quad (4)$$

For this age-by-cognition interaction analysis, we included both the observations from baseline and 2-year follow-up of the ABCD dataset and utilized baseline fluid cognition as the by-item to fit GAMM models. Using the acquired models, we estimated structural connectivity strength by assigning cognitive performance as low and high levels respectively. To define these levels, we used the 10th percentile of baseline cognitive performance for the low level, and the 90th percentile for the high level. We then averaged trajectories for low and high cognition levels independently within deciles of the S-A connectional axis for visualization purposes.

Psychopathological associations with structural connectivity strength

We further evaluated the associations between the general psychopathological factor, *p*-factor, and structural connectivity strength. These psychopathological analyses were conducted only in the ABCD dataset, as the ABCD study included participants with various psychiatric disorders diagnoses. The associations were evaluated through GAMMs while controlling age, sex, and mean FD. See below for the equation (5).

$$\text{Structural connectivity strength} \sim p\text{-factor} + s(\text{Age}, k = 3) + \text{Sex} + \text{Mean\_FD} \quad (5)$$

Similar to cognitive analysis, the *T* value of the structural connectivity strength term indicates the magnitude and direction of the association between fluid cognition and structural connectivity, and its significance was determined by comparing the full model with a null model lacking the *p*-factor term. GAMM comparisons employed a parametric bootstrap method utilizing the likelihood ratio test statistic with 1,000 simulations, supported by the *pbkrtest* package(Halekoh and Højsgaard, 2014). FDR correction was utilized to adjust *P* values. To evaluate the alignment of psychopathological associations with the S-A connectional axis rank, we performed Spearman's

rank correlation analysis.

Subsequently, we further depicted the developmental trajectories by different levels of *p*-factors to elucidate how developmental trajectories of structural connectivity strength differed between individuals with varying severity of general psychiatric symptoms. To achieve this, we modeled age-dependent changes in structural connectivity strength as a function of *p*-factors (see equation (6)).

$$\text{Structural connectivity strength} \sim s(\text{Age, by} = p\text{-factor}, k = 3) + s(\text{Age}, k = 3) + \text{Sex} + \text{Mean\_FD} \quad (6)$$

Based on this model, we estimated structural connectivity strength by assigning *p*-factor as low and high levels respectively. To define these levels, we used the 10th percentile of the p-factor for the low level, which represents no or mild psychiatric symptoms, and the 90th percentile for the high level, which represents severe psychiatric symptoms. We then averaged trajectories for low and high *p*-factor levels independently within deciles of the S-A connectional axis for visualization purposes.

Correction for multi-site batch effects

Data in the HCP-D and ABCD datasets were collected from multi-acquisition sites. The ComBat harmonization technique has been shown to be effective in reducing batch effects in neuroimaging studies(Fortin et al., 2017; Middleton et al., 2023). In this study, we applied the ComBat method using an empirical Bayes framework(Johnson et al., 2007; Larsen et al., 2020) on each of the 78 connections with acquisition sites as the batch effect. Additionally, age, sex and mean FD were included as covariates, where age was modeled as a smooth term using GAM or GAMM. For cognitive and psychopathological analyses, fluid cognition and the *p*-factor were also included in models, so these two variables were additionally added as covariates separately in the ComBat processing for these analyses.

Sensitivity analyses

We performed a series of sensitivity analyses to ascertain the robustness of our findings. The first sensitive analysis aimed to test whether the resolution of large-scale structural connectome would affect the results. Rather than parcellating the cortex into 12 cortical systems, we acquired a cortical parcellation of 7 or 17 systems. We next computed the structural connectome with 28 connections among 7 systems, as well the connectome with 153 connections among 17 systems, per scan. We next repeated all the analyses with the connectome of these two resolutions.

Second, as the Euclidean distance between regions could impact the structural connectivity strength, we evaluated whether this distance would confound our findings. To do this, we regressed the Euclidean distance of pairwise systems in the MNI space from the acquired effect size matrix of age, cognitive, and psychopathological effects of structural connectivity strength.

Third, we examined whether our findings were confounded by socioeconomic status (SES) or intracranial volume (ICV). SES was measured by the family income-to-needs ratio as prior research(Barch et al., 2022; King et al., 2020). The family income-to-needs ratio was computed as the annual family income divided by the federal poverty line from the Federal Register by the U.S. Department of Health and Human Services (https://aspe.hhs.gov/topics/poverty-economic-mobility/poverty-guidelines/prior-hhs-poverty-guidelines-federal-register-references). The intracranial volume was computed via *FreeSurfer*. Individuals' SES or ICV were added as additional covariates when evaluating the associations between structural connectivity strength and age, cognition, or psychopathology.

Data and code availability

The HCP-Development 2.0 Release data used in this report came from DOI: 10.15154/1520708 via the NDA (https://nda.nih.gov/ccf). The ABCD 5.1 data release used in this report came from DOI: 10.15154/z563-zd24 via the NDA (https://nda.nih.gov/abcd). The fast-track data from the ABCD Study data is also available through the NDA. All analysis methods are described in the main text and supplementary materials. All codes used to perform the analyses in this study and the statistical magnitudes derived from analyses can be found at https://github.com/CuiLabCIBR/SCDevelopment.git. All analysis methods are described in the main text and supplementary materials.

Acknowledgments

We thank the research participants and staff involved in data collection of The Lifespan Human Connectome Project Development (HCP-D) study and Adolescent Brain Cognitive Development (ABCD) Study. The HCP-D data were provided by the Human Connectome Project, WU-Minn Consortium (Principal Investigators: David Van Essen and Kamil Ugurbil; 1U54MH091657) funded by the 16 National Institutes of Health (NIH) Institutes and Centers that support the NIH Blueprint for Neuroscience Research; and by the McDonnell Center for Systems Neuroscience at Washington University. Research reported in this publication was supported by the National Institute of Mental Health of NIH under Award Number U01MH109589 and by funds provided by the McDonnell Center for Systems Neuroscience at Washington University in St. Louis. The ABCD data were provided by the ABCD Study (abcdstudy.org) funded by NIH. The ABCD Study is a multisite, longitudinal study designed to recruit more than 10,000 children ages 9-10 years old and follow them over 10 years into early adulthood. The ABCD Study is supported by the NID and additional federal partners under award numbers U01DA041048, U01DA050989, U01DA051016, U01DA041022, U01DA051018, U01DA051037, U01DA050987, U01DA041174, U01DA041106, U01DA041117, U01DA041028, U01DA041134, U01DA050988, U01DA051039, U01DA041156, U01DA041025, U01DA041120, U01DA051038, U01DA041148, U01DA041093, U01DA041089, U24DA041123 and U24DA041147. A full list of supporters is available at https://abcdstudy.org/federal-

partners.html. A listing of participating sites and a complete listing of the study investigators can be found at https://abcdstudy.org/consortium_members/. ABCD consortium investigators designed and implemented the study and/or provided data but did not necessarily participate in the analysis or writing of this report. This manuscript reflects the views of the authors and may not reflect the opinions or views of the NIH or ABCD consortium investigators. The ABCD data repository grows and changes over time. **Funding:** This work was supported by the STI 2030-Major Projects (grant number 2022ZD0211300), Beijing Nova Program (grant number Z211100002121002), Chinese Institute for Brain Research, Beijing (CIBR) funds. V.J.S. is supported by the National Institute of Mental Health, USA (grant number T32MH016804).

Author contributions

Z.C. and X.X. conceptualized the study. X.X., H.Y., and J.C. curated the data. X.X. conducted the formal analysis. X.X. and H.Y. created the visualizations. J.C. replicated all analyses. Z.C. managed the project administration and supervised the project. X.X. and Z.C. wrote the original draft. V.J.S. commented on analyses. Z.C., X.X., H.Y., J.C., and V.J.S. reviewed and edited the manuscript.

Declaration of interests

The authors declare no competing interests.

Supplemental information

Supplementary Text

Figures S1 to S8

Tables S1 to S2

Materials and correspondence

Further information and requests for resources should be directed to and will be fulfilled by the Contact, Zaixu Cui (cuizaixu@cibr.ac.cn).

References

Achenbach, T.M., and Verhulst, F. (2009). The Achenbach System of Empirically Based Assessment (ASEBA): Development, Findings, Theory, and Applications.

Akshoomoff, N., Beaumont, J.L., Bauer, P.J., Dikmen, S.S., Gershon, R.C., Mungas, D., Slotkin, J., Tulsky, D., Weintraub, S., Zelazo, P.D., and Heaton, R.K. (2013). VIII. NIH Toolbox Cognition Battery (CB): composite scores of crystallized, fluid, and overall cognition. Monogr Soc Res Child Dev *78*, 119-132. 10.1111/mono.12038.

Andersson, J.L.R., Graham, M.S., Zsoldos, E., and Sotiropoulos, S.N. (2016). Incorporating outlier detection and replacement into a non-parametric framework for movement and distortion correction of diffusion MR images. Neuroimage *141*, 556-572. 10.1016/j.neuroimage.2016.06.058.

Bagautdinova, J., Bourque, J., Sydnor, V.J., Cieslak, M., Alexander-Bloch, A.F., Bertolero, M.A., Cook, P.A., Gur, R.E., Gur, R.C., Hu, F., et al. (2023). Development of white matter fiber covariance networks supports executive function in youth. Cell Rep *42*, 113487. 10.1016/j.celrep.2023.113487.

Barch, D.M., Donohue, M.R., Elsayed, N.M., Gilbert, K., Harms, M.P., Hennefield, L., Herzberg, M., Kandala, S., Karcher, N.R., Jackson, J.J., et al. (2022). Early Childhood Socioeconomic Status and Cognitive and Adaptive Outcomes at the Transition to Adulthood: The Mediating Role of Gray Matter Development Across Five Scan Waves. Biological Psychiatry: Cognitive Neuroscience and Neuroimaging *7*, 34-44. https://doi.org/10.1016/j.bpsc.2021.07.002.

Baum, G.L., Ciric, R., Roalf, D.R., Betzel, R.F., Moore, T.M., Shinohara, R.T., Kahn, A.E., Vandekar, S.N., Rupert, P.E., Quarmley, M., et al. (2017). Modular Segregation of Structural Brain Networks Supports the Development of Executive Function in Youth. Curr Biol. *27*, 1561-1572 e1568. 10.1016/j.cub.2017.04.051.

Baum, G.L., Cui, Z., Roalf, D.R., Ciric, R., Betzel, R.F., Larsen, B., Cieslak, M., Cook, P.A., Xia, C.H., Moore, T.M., et al. (2020). Development of structure-function coupling in human brain networks during youth. Proc Natl Acad Sci U S A *117*, 771-778. 10.1073/pnas.1912034117.

Baum, G.L., Flournoy, J.C., Glasser, M.F., Harms, M.P., Mair, P., Sanders, A.F.P., Barch, D.M., Buckner, R.L., Bookheimer, S., Dapretto, M., et al. (2022). Graded Variation in T1w/T2w Ratio during Adolescence: Measurement, Caveats, and Implications for Development of Cortical Myelin. The Journal of neuroscience : the official journal of the Society for Neuroscience *42*, 5681-5694. 10.1523/JNEUROSCI.2380-21.2022.

Bethlehem, R.A.I., Seidlitz, J., White, S.R., Vogel, J.W., Anderson, K.M., Adamson, C., Adler, S., Alexopoulos, G.S., Anagnostou, E., Areces-Gonzalez, A., et al. (2022). Brain charts for the human lifespan. Nature *604*, 525-533. 10.1038/s41586-022-04554-y.

Cammoun, L., Gigandet, X., Meskaldji, D., Thiran, J.P., Sporns, O., Do, K.Q., Maeder, P., Meuli, R., and Hagmann, P. (2012). Mapping the human connectome at multiple scales with diffusion spectrum MRI. J Neurosci Methods *203*, 386-397. 10.1016/j.jneumeth.2011.09.031.

Casey, B.J., Cannonier, T., Conley, M.I., Cohen, A.O., Barch, D.M., Heitzeg, M.M., Soules, M.E., Teslovich, T., Dellarco, D.V., Garavan, H., et al. (2018). The Adolescent Brain Cognitive Development (ABCD) study: Imaging acquisition across 21 sites. Developmental cognitive

neuroscience *32*, 43-54. 10.1016/j.dcn.2018.03.001.
Caspi, A., and Moffitt, T.E. (2018). All for One and One for All: Mental Disorders in One Dimension. Am J Psychiatry *175*, 831-844. 10.1176/appi.ajp.2018.17121383.
Chen, H., Liu, T., Zhao, Y., Zhang, T., Li, Y., Li, M., Zhang, H., Kuang, H., Guo, L., Tsien, J.Z., and Liu, T. (2015). Optimization of large-scale mouse brain connectome via joint evaluation of DTI and neuron tracing data. NeuroImage *115*, 202-213. 10.1016/j.neuroimage.2015.04.050.
Chereau, R., Saraceno, G.E., Angibaud, J., Cattaert, D., and Nagerl, U.V. (2017). Superresolution imaging reveals activity-dependent plasticity of axon morphology linked to changes in action potential conduction velocity. Proc Natl Acad Sci U S A *114*, 1401-1406. 10.1073/pnas.1607541114.
Cieslak, M., Cook, P.A., He, X., Yeh, F.C., Dhollander, T., Adebimpe, A., Aguirre, G.K., Bassett, D.S., Betzel, R.F., Bourque, J., et al. (2021). QSIPrep: an integrative platform for preprocessing and reconstructing diffusion MRI data. Nat Methods *18*, 775-778. 10.1038/s41592-021-01185-5.
Concha, L., Gross, D.W., and Beaulieu, C. (2005). Diffusion tensor tractography of the limbic system. AJNR. American journal of neuroradiology *26*, 2267-2274.
Cui, Z., Li, H., Xia, C.H., Larsen, B., Adebimpe, A., Baum, G.L., Cieslak, M., Gur, R.E., Gur, R.C., Moore, T.M., et al. (2020). Individual Variation in Functional Topography of Association Networks in Youth. Neuron *106*, 340-353. 10.1016/j.neuron.2020.01.029.
de Faria, O., Jr., Pivonkova, H., Varga, B., Timmler, S., Evans, K.A., and Karadottir, R.T. (2021). Periods of synchronized myelin changes shape brain function and plasticity. Nat Neurosci *24*, 1508-1521. 10.1038/s41593-021-00917-2.
Donahue, C.J., Sotiropoulos, S.N., Jbabdi, S., Hernandez-Fernandez, M., Behrens, T.E., Dyrby, T.B., Coalson, T., Kennedy, H., Knoblauch, K., Van Essen, D.C., and Glasser, M.F. (2016). Using Diffusion Tractography to Predict Cortical Connection Strength and Distance: A Quantitative Comparison with Tracers in the Monkey. The Journal of neuroscience : the official journal of the Society for Neuroscience *36*, 6758-6770. 10.1523/jneurosci.0493-16.2016.
Ebesutani, C., Bernstein, A., Nakamura, B.J., Chorpita, B.F., Higa-McMillan, C.K., Weisz, J.R., and The Research Network on Youth Mental, H. (2010). Concurrent Validity of the Child Behavior Checklist DSM-Oriented Scales: Correspondence with DSM Diagnoses and Comparison to Syndrome Scales. J Psychopathol Behav Assess *32*, 373-384. 10.1007/s10862-009-9174-9.
Edition, F. (2013). Diagnostic and statistical manual of mental disorders. Am Psychiatric Assoc *21*.
Fields, R.D. (2015). A new mechanism of nervous system plasticity: activity-dependent myelination. Nat Rev Neurosci *16*, 756-767. 10.1038/nrn4023.
Finc, K., Bonna, K., He, X., Lydon-Staley, D.M., Kuhn, S., Duch, W., and Bassett, D.S. (2020). Dynamic reconfiguration of functional brain networks during working memory training. Nat Commun *11*, 2435. 10.1038/s41467-020-15631-z.
Fischl, B. (2012). FreeSurfer. Neuroimage *62*, 774-781. 10.1016/j.neuroimage.2012.01.021.
Fortin, J.P., Parker, D., Tunc, B., Watanabe, T., Elliott, M.A., Ruparel, K., Roalf, D.R., Satterthwaite, T.D., Gur, R.C., Gur, R.E., et al. (2017). Harmonization of multi-site diffusion tensor imaging data. NeuroImage *161*, 149-170. 10.1016/j.neuroimage.2017.08.047.
Garavan, H., Bartsch, H., Conway, K., Decastro, A., Goldstein, R.Z., Heeringa, S., Jernigan, T.,

Potter, A., Thompson, W., and Zahs, D. (2018). Recruiting the ABCD sample: Design considerations and procedures. Developmental cognitive neuroscience *32*, 16-22. 10.1016/j.dcn.2018.04.004.

Garyfallidis, E., Brett, M., Amirbekian, B., Rokem, A., van der Walt, S., Descoteaux, M., Nimmo-Smith, I., and Dipy, C. (2014). Dipy, a library for the analysis of diffusion MRI data. Front Neuroinform *8*, 8. 10.3389/fninf.2014.00008.

Ge, J., Yang, G., Han, M., Zhou, S., Men, W., Qin, L., Lyu, B., Li, H., Wang, H., Rao, H., et al. (2023). Increasing diversity in connectomics with the Chinese Human Connectome Project. Nat Neurosci *26*, 163-172. 10.1038/s41593-022-01215-1.

Girard, G., Caminiti, R., Battaglia-Mayer, A., St-Onge, E., Ambrosen, K.S., Eskildsen, S.F., Krug, K., Dyrby, T.B., Descoteaux, M., Thiran, J.P., and Innocenti, G.M. (2020). On the cortical connectivity in the macaque brain: A comparison of diffusion tractography and histological tracing data. NeuroImage *221*, 117201. 10.1016/j.neuroimage.2020.117201.

Glasser, M.F., Sotiropoulos, S.N., Wilson, J.A., Coalson, T.S., Fischl, B., Andersson, J.L., Xu, J., Jbabdi, S., Webster, M., Polimeni, J.R., et al. (2013). The minimal preprocessing pipelines for the Human Connectome Project. NeuroImage *80*, 105-124. 10.1016/j.neuroimage.2013.04.127.

Gordon, E.M., Laumann, T.O., Gilmore, A.W., Newbold, D.J., Greene, D.J., Berg, J.J., Ortega, M., Hoyt-Drazen, C., Gratton, C., Sun, H., et al. (2017). Precision Functional Mapping of Individual Human Brains. Neuron *95*, 791-807 e797. 10.1016/j.neuron.2017.07.011.

Greene, D.J., Koller, J.M., Hampton, J.M., Wesevich, V., Van, A.N., Nguyen, A.L., Hoyt, C.R., McIntyre, L., Earl, E.A., Klein, R.L., et al. (2018). Behavioral interventions for reducing head motion during MRI scans in children. NeuroImage *171*, 234-245. 10.1016/j.neuroimage.2018.01.023.

Hagler, D.J., Jr., Hatton, S., Cornejo, M.D., Makowski, C., Fair, D.A., Dick, A.S., Sutherland, M.T., Casey, B.J., Barch, D.M., Harms, M.P., et al. (2019). Image processing and analysis methods for the Adolescent Brain Cognitive Development Study. NeuroImage *202*, 116091. 10.1016/j.neuroimage.2019.116091.

Hagmann, P., Cammoun, L., Gigandet, X., Meuli, R., Honey, C.J., Wedeen, V.J., and Sporns, O. (2008). Mapping the structural core of human cerebral cortex. PLoS Biol *6*, e159. 10.1371/journal.pbio.0060159.

Halekoh, U., and Højsgaard, S. (2014). A kenward-roger approximation and parametric bootstrap methods for tests in linear mixed models–the R package pbkrtest. Journal of Statistical Software *59*, 1-32.

Harms, M.P., Somerville, L.H., Ances, B.M., Andersson, J., Barch, D.M., Bastiani, M., Bookheimer, S.Y., Brown, T.B., Buckner, R.L., Burgess, G.C., et al. (2018). Extending the Human Connectome Project across ages: Imaging protocols for the Lifespan Development and Aging projects. NeuroImage *183*, 972-984. 10.1016/j.neuroimage.2018.09.060.

Hermosillo, R.J.M., Moore, L.A., Feczko, E., Miranda-Domínguez, Ó., Pines, A., Dworetsky, A., Conan, G., Mooney, M.A., Randolph, A., Graham, A., et al. (2024). A precision functional atlas of personalized network topography and probabilities. Nature Neuroscience. 10.1038/s41593-024-01596-5.

Hu, L.t., and Bentler, P.M. (1999). Cutoff criteria for fit indexes in covariance structure analysis: Conventional criteria versus new alternatives. Structural Equation Modeling: A Multidisciplinary Journal *6*, 1-55. 10.1080/10705519909540118.

Insel, T.R. (2014a). Mental disorders in childhood: shifting the focus from behavioral symptoms to neurodevelopmental trajectories. Jama *311*, 1727-1728. 10.1001/jama.2014.1193.

Insel, T.R. (2014b). The NIMH Research Domain Criteria (RDoC) Project: precision medicine for psychiatry. Am J Psychiatry *171*, 395-397. 10.1176/appi.ajp.2014.14020138.

Jenkinson, M., Beckmann, C.F., Behrens, T.E.J., Woolrich, M.W., and Smith, S.M. (2012). FSL. NeuroImage *62*, 782-790. https://doi.org/10.1016/j.neuroimage.2011.09.015.

Jeurissen, B., Tournier, J.-D., Dhollander, T., Connelly, A., and Sijbers, J. (2014). Multi-tissue constrained spherical deconvolution for improved analysis of multi-shell diffusion MRI data. NeuroImage *103*, 411-426. 10.1016/j.neuroimage.2014.07.061.

Johnson, W.E., Li, C., and Rabinovic, A. (2007). Adjusting batch effects in microarray expression data using empirical Bayes methods. Biostatistics *8*, 118-127. 10.1093/biostatistics/kxj037.

Keller, A.S., Pines, A.R., Shanmugan, S., Sydnor, V.J., Cui, Z., Bertolero, M.A., Barzilay, R., Alexander-Bloch, A.F., Byington, N., Chen, A., et al. (2023a). Personalized functional brain network topography is associated with individual differences in youth cognition. Nat Commun *14*, 8411. 10.1038/s41467-023-44087-0.

Keller, A.S., Sydnor, V.J., Pines, A., Fair, D.A., Bassett, D.S., and Satterthwaite, T.D. (2023b). Hierarchical functional system development supports executive function. Trends Cogn Sci *27*, 160-174. 10.1016/j.tics.2022.11.005.

Kellner, E., Dhital, B., Kiselev, V.G., and Reisert, M. (2016). Gibbs-ringing artifact removal based on local subvoxel-shifts. Magnetic resonance in medicine : official journal of the Society of Magnetic Resonance in Medicine / Society of Magnetic Resonance in Medicine *76*, 1574-1581. 10.1002/mrm.26054.

King, L.S., Dennis, E.L., Humphreys, K.L., Thompson, P.M., and Gotlib, I.H. (2020). Cross-sectional and longitudinal associations of family income-to-needs ratio with cortical and subcortical brain volume in adolescent boys and girls. Developmental cognitive neuroscience *44*, 100796.

Kotov, R., Krueger, R.F., Watson, D., Achenbach, T.M., Althoff, R.R., Bagby, R.M., Brown, T.A., Carpenter, W.T., Caspi, A., Clark, L.A., et al. (2017). The Hierarchical Taxonomy of Psychopathology (HiTOP): A dimensional alternative to traditional nosologies. J Abnorm Psychol *126*, 454-477. 10.1037/abn0000258.

Larsen, B., Bourque, J., Moore, T.M., Adebimpe, A., Calkins, M.E., Elliott, M.A., Gur, R.C., Gur, R.E., Moberg, P.J., Roalf, D.R., et al. (2020). Longitudinal Development of Brain Iron Is Linked to Cognition in Youth. The Journal of neuroscience : the official journal of the Society for Neuroscience *40*, 1810-1818. 10.1523/JNEUROSCI.2434-19.2020.

Larsen, B., and Luna, B. (2018). Adolescence as a neurobiological critical period for the development of higher-order cognition. Neuroscience and biobehavioral reviews *94*, 179-195. 10.1016/j.neubiorev.2018.09.005.

Lawes, I.N., Barrick, T.R., Murugam, V., Spierings, N., Evans, D.R., Song, M., and Clark, C.A.

(2008). Atlas-based segmentation of white matter tracts of the human brain using diffusion tensor tractography and comparison with classical dissection. NeuroImage *39*, 62-79. 10.1016/j.neuroimage.2007.06.041.

Le Bihan, D. (2003). Looking into the functional architecture of the brain with diffusion MRI. Nat. Rev. Neurosci. *4*, 469-480.

Lebel, C., and Beaulieu, C. (2011). Longitudinal development of human brain wiring continues from childhood into adulthood. The Journal of neuroscience : the official journal of the Society for Neuroscience *31*, 10937-10947. 10.1523/jneurosci.5302-10.2011.

Lebel, C., Treit, S., and Beaulieu, C. (2019). A review of diffusion MRI of typical white matter development from early childhood to young adulthood. NMR in biomedicine *32*, e3778. 10.1002/nbm.3778.

Luo, A.C., Sydnor, V.J., Pines, A., Larsen, B., Alexander-Bloch, A.F., Cieslak, M., Covitz, S., Chen, A.A., Esper, N.B., Feczko, E., et al. (2024). Functional connectivity development along the sensorimotor-association axis enhances the cortical hierarchy. Nature Communications *15*. 10.1038/s41467-024-47748-w.

Maier-Hein, K.H., Neher, P.F., Houde, J.C., Cote, M.A., Garyfallidis, E., Zhong, J., Chamberland, M., Yeh, F.C., Lin, Y.C., Ji, Q., et al. (2017). The challenge of mapping the human connectome based on diffusion tractography. Nat Commun *8*, 1349. 10.1038/s41467-017-01285-x.

Marcus, D.S., Harwell, J., Olsen, T., Hodge, M., Glasser, M.F., Prior, F., Jenkinson, M., Laumann, T., Curtiss, S.W., and Van Essen, D.C. (2011). Informatics and data mining tools and strategies for the human connectome project. Front Neuroinform *5*, 4. 10.3389/fninf.2011.00004.

McFadyen, J., Dolan, R.J., and Garrido, M.I. (2020). The influence of subcortical shortcuts on disordered sensory and cognitive processing. Nat Rev Neurosci *21*, 264-276. 10.1038/s41583-020-0287-1.

Menon, V., and D'Esposito, M. (2022). The role of PFC networks in cognitive control and executive function. Neuropsychopharmacology *47*, 90-103. 10.1038/s41386-021-01152-w.

Middleton, D.M., Li, Y., Chen, A., Shinohara, R., Fisher, J., Krisa, L., Elliot, M., Faro, S.H., Woo, J.H., Flanders, A.E., and Mohamed, F.B. (2023). Harmonization of multi-site diffusion tensor imaging data for cervical and thoracic spinal cord at 1.5 T and 3 T using longitudinal ComBat. Sci Rep *13*, 19809. 10.1038/s41598-023-46465-6.

Moore, T.M., Kaczkurkin, A.N., Durham, E.L., Jeong, H.J., McDowell, M.G., Dupont, R.M., Applegate, B., Tackett, J.L., Cardenas-Iniguez, C., Kardan, O., et al. (2020). Criterion validity and relationships between alternative hierarchical dimensional models of general and specific psychopathology. J Abnorm Psychol *129*, 677-688. 10.1037/abn0000601.

Muthén, L.K., and Muthén, B.O. (2017). Mplus User's Guide., Eighth Edition. Edition.

Pines, A.R., Cieslak, M., Larsen, B., Baum, G.L., Cook, P.A., Adebimpe, A., Dávila, D.G., Elliott, M.A., Jirsaraie, R., Murtha, K., et al. (2020). Leveraging multi-shell diffusion for studies of brain development in youth and young adulthood. Developmental cognitive neuroscience *43*, 100788. 10.1016/j.dcn.2020.100788.

Pines, A.R., Larsen, B., Cui, Z., Sydnor, V.J., Bertolero, M.A., Adebimpe, A., Alexander-Bloch, A.F., Davatzikos, C., Fair, D.A., Gur, R.C., et al. (2022). Dissociable multi-scale patterns of

development in personalized brain networks. Nat Commun *13*, 2647. 10.1038/s41467-022-30244-4.

Power, J.D., Cohen, A.L., Nelson, S.M., Wig, G.S., Barnes, K.A., Church, J.A., Vogel, A.C., Laumann, T.O., Miezin, F.M., Schlaggar, B.L., and Petersen, S.E. (2011). Functional Network Organization of the Human Brain. Neuron *72*, 665-678. 10.1016/j.neuron.2011.09.006.

Power, J.D., Mitra, A., Laumann, T.O., Snyder, A.Z., Schlaggar, B.L., and Petersen, S.E. (2014). Methods to detect, characterize, and remove motion artifact in resting state fMRI. NeuroImage *84*, 320-341. https://doi.org/10.1016/j.neuroimage.2013.08.048.

Riccomagno, M.M., and Kolodkin, A.L. (2015). Sculpting neural circuits by axon and dendrite pruning. Annu Rev Cell Dev Biol *31*, 779-805. 10.1146/annurev-cellbio-100913-013038.

Roberts, J.A., Perry, A., Roberts, G., Mitchell, P.B., and Breakspear, M. (2017). Consistency-based thresholding of the human connectome. NeuroImage *145*, 118-129. 10.1016/j.neuroimage.2016.09.053.

Sampaio-Baptista, C., and Johansen-Berg, H. (2017). White Matter Plasticity in the Adult Brain. Neuron *96*, 1239-1251. 10.1016/j.neuron.2017.11.026.

Schaefer, A., Kong, R., Gordon, E.M., Laumann, T.O., Zuo, X.N., Holmes, A.J., Eickhoff, S.B., and Yeo, B.T.T. (2018). Local-Global Parcellation of the Human Cerebral Cortex from Intrinsic Functional Connectivity MRI. Cerebral cortex (New York, N.Y. : 1991) *28*, 3095-3114. 10.1093/cercor/bhx179.

Shen, K.K., Welton, T., Lyon, M., McCorkindale, A.N., Sutherland, G.T., Burnham, S., Fripp, J., Martins, R., and Grieve, S.M. (2020). Structural core of the executive control network: A high angular resolution diffusion MRI study. Human brain mapping *41*, 1226-1236. 10.1002/hbm.24870.

Simpson, G.L. (2021). gratia: Graceful 'ggplot'-based graphics and other functions for GAMs fitted using 'mgcv'. R package version 0.6. 0.

Smith, R., Skoch, A., Bajada, C.J., Caspers, S., and Connelly, A. (2020). Hybrid surface-volume segmentation for improved anatomically-constrained tractography.

Smith, R.E., Tournier, J.-D., Calamante, F., and Connelly, A. (2012). Anatomically-constrained tractography: improved diffusion MRI streamlines tractography through effective use of anatomical information. NeuroImage *62*, 1924-1938. 10.1016/j.neuroimage.2012.06.005.

Smith, R.E., Tournier, J.-D., Calamante, F., and Connelly, A. (2015a). SIFT2: Enabling dense quantitative assessment of brain white matter connectivity using streamlines tractography. NeuroImage *119*, 338-351. 10.1016/j.neuroimage.2015.06.092.

Smith, R.E., Tournier, J.D., Calamante, F., and Connelly, A. (2015b). SIFT2: Enabling dense quantitative assessment of brain white matter connectivity using streamlines tractography. NeuroImage *119*, 338-351. 10.1016/j.neuroimage.2015.06.092.

Sokolov, A.A., Miall, R.C., and Ivry, R.B. (2017). The Cerebellum: Adaptive Prediction for Movement and Cognition. Trends Cogn Sci *21*, 313-332. 10.1016/j.tics.2017.02.005.

Somerville, L.H., Bookheimer, S.Y., Buckner, R.L., Burgess, G.C., Curtiss, S.W., Dapretto, M., Elam, J.S., Gaffrey, M.S., Harms, M.P., Hodge, C., et al. (2018). The Lifespan Human Connectome Project in Development: A large-scale study of brain connectivity development in 5-21 year olds.

NeuroImage *183*, 456-468. 10.1016/j.neuroimage.2018.08.050.

Sotiropoulos, S.N., and Zalesky, A. (2019). Building connectomes using diffusion MRI: why, how and but. NMR in biomedicine *32*, e3752. 10.1002/nbm.3752.

Sporns, O., Tononi, G., and Kotter, R. (2005). The human connectome: A structural description of the human brain. PLoS Comput Biol *1*, e42. 10.1371/journal.pcbi.0010042.

Sydnor, V.J., Larsen, B., Bassett, D.S., Alexander-Bloch, A., Fair, D.A., Liston, C., Mackey, A.P., Milham, M.P., Pines, A., Roalf, D.R., et al. (2021). Neurodevelopment of the association cortices: Patterns, mechanisms, and implications for psychopathology. Neuron *109*, 2820-2846. 10.1016/j.neuron.2021.06.016.

Sydnor, V.J., Larsen, B., Seidlitz, J., Adebimpe, A., Alexander-Bloch, A.F., Bassett, D.S., Bertolero, M.A., Cieslak, M., Covitz, S., Fan, Y., et al. (2023). Intrinsic activity development unfolds along a sensorimotor-association cortical axis in youth. Nat Neurosci. 10.1038/s41593-023-01282-y.

Thiebaut de Schotten, M., and Forkel, S.J. (2022). The emergent properties of the connected brain. Science (New York, N.Y.) *378*, 505-510. 10.1126/science.abq2591.

Tournier, J.D., Calamante, F., and Connelly, A. (2010). Improved probabilistic streamlines tractography by 2nd order integration over fibre orientation distributions. (John Wiley & Sons, Inc New Jersey, USA).

Tournier, J.D., Smith, R., Raffelt, D., Tabbara, R., Dhollander, T., Pietsch, M., Christiaens, D., Jeurissen, B., Yeh, C.H., and Connelly, A. (2019). MRtrix3: A fast, flexible and open software framework for medical image processing and visualisation. NeuroImage *202*, 116137. 10.1016/j.neuroimage.2019.116137.

Tustison, N.J., Avants, B.B., Cook, P.A., Zheng, Y., Egan, A., Yushkevich, P.A., and Gee, J.C. (2010). N4ITK: improved N3 bias correction. IEEE transactions on medical imaging *29*, 1310-1320. 10.1109/TMI.2010.2046908.

van den Heuvel, M.P., de Reus, M.A., Feldman Barrett, L., Scholtens, L.H., Coopmans, F.M., Schmidt, R., Preuss, T.M., Rilling, J.K., and Li, L. (2015). Comparison of diffusion tractography and tract-tracing measures of connectivity strength in rhesus macaque connectome. Human brain mapping *36*, 3064-3075. 10.1002/hbm.22828.

Veraart, J., Novikov, D.S., Christiaens, D., Ades-Aron, B., Sijbers, J., and Fieremans, E. (2016). Denoising of diffusion MRI using random matrix theory. Neuroimage *142*, 394-406. 10.1016/j.neuroimage.2016.08.016.

Wang, D., Buckner, R.L., Fox, M.D., Holt, D.J., Holmes, A.J., Stoecklein, S., Langs, G., Pan, R., Qian, T., Li, K., et al. (2015). Parcellating cortical functional networks in individuals. Nat Neurosci *18*, 1853-1860. 10.1038/nn.4164.

Warton, D.I. (2022). Eco-stats: Data analysis in ecology. Cham, Switzerland: Springer Nature Switzerland AG.

Weintraub, S., Dikmen, S.S., Heaton, R.K., Tulsky, D.S., Zelazo, P.D., Bauer, P.J., Carlozzi, N.E., Slotkin, J., Blitz, D., and Wallner-Allen, K. (2013). Cognition assessment using the NIH Toolbox. Neurology *80*, S54-S64.

Wood, S. (2014). gamm4: Generalized additive mixed models using mgcv and lme4. R Packag. version 0.2-3 *version 0.2-3*.

Wood, S.N. (2017). Generalized additive models: an introduction with R (CRC press).

Xia, C.H., Ma, Z., Ciric, R., Gu, S., Betzel, R.F., Kaczkurkin, A.N., Calkins, M.E., Cook, P.A., Garcia de la Garza, A., Vandekar, S.N., et al. (2018). Linked dimensions of psychopathology and connectivity in functional brain networks. Nat Commun *9*, 3003. 10.1038/s41467-018-05317-y.

Yarkoni, T. (2009). Big Correlations in Little Studies: Inflated fMRI Correlations Reflect Low Statistical Power-Commentary on Vul et al. (2009). Perspect Psychol Sci *4*, 294-298. 10.1111/j.1745-6924.2009.01127.x.

Yeh, F.C., Verstynen, T.D., Wang, Y., Fernandez-Miranda, J.C., and Tseng, W.Y. (2013). Deterministic diffusion fiber tracking improved by quantitative anisotropy. PloS one *8*, e80713. 10.1371/journal.pone.0080713.

Yendiki, A., Aggarwal, M., Axer, M., Howard, A.F.D., van Walsum, A.V.C., and Haber, S.N. (2022). Post mortem mapping of connectional anatomy for the validation of diffusion MRI. NeuroImage *256*, 119146. 10.1016/j.neuroimage.2022.119146.

Yeo, B.T., Krienen, F.M., Sepulcre, J., Sabuncu, M.R., Lashkari, D., Hollinshead, M., Roffman, J.L., Smoller, J.W., Zollei, L., Polimeni, J.R., et al. (2011). The organization of the human cerebral cortex estimated by intrinsic functional connectivity. J Neurophysiol *106*, 1125-1165. 10.1152/jn.00338.2011.

Yu, Q., Guan, T., Guo, Y., and Kong, J. (2023). The Initial Myelination in the Central Nervous System. ASN Neuro *15*, 17590914231163039. 10.1177/17590914231163039.